©2004 by Economic Geology
Vol. 99, pp. 1063–1084

The Hemlo Gold Deposit, Ontario: An Example of Melting and Mobilization of a Precious Metal-Sulfosalt Assemblage during Amphibolite Facies Metamorphism and Deformation

Andrew G. Tomkins,†

Department of Geology and Geophysics, University of Calgary, Calgary, Alberta, Canada T2N 1N4

David R. M. Pattison,

Department of Geology and Geophysics, University of Calgary, Calgary, Alberta, Canada T2N 1N4

and Eva Zaleski

Geological Survey of Canada, 3303 – 33rd St. NW, Calgary, Alberta, Canada T2L 2A7

Abstract

The timing of mineralization at the Hemlo gold deposit has long been a controversial issue. We present arguments that use partial melting of the ore assemblage to explain the mechanism of ore mobilization and resolve problems with the model of premetamorphic mineralization. The results have implications for mine exploitation and exploration strategies. We show that the ore mineral assemblage underwent partial melting during middle-amphibolite facies metamorphism (600°–650°C, 6–7 kbars), primarily through breakdown of stibnite and arsenopyrite in a high-f_{S_2} environment. Concurrent deformation led to segregation of the resulting Sb- and As-rich sulfosalt melt. Interaction between this melt and a range of unmelted sulfides led to further melting and incorporation of other elements into the melt. The gold-bearing melt was mobilized from compressional high-strain sites into dilational domains such as boudin necks and extensional fractures developed in competent lithologies. Ore minerals that did not melt significantly (pyrite, molybdenite, pyrrhotite, and sphalerite) were not extensively mobilized and largely remained within high-strain compressional domains. This segregation of melt from residue thus resulted in the observed heterogeneous distribution of ore minerals within the deposit. Crystallization of the sulfosalt melt produced a diverse suite of ore minerals, dominated by stibnite and realgar and containing an array of rare sulfosalts, native elements, intermetallic compounds, and tellurides. Some sulfosalt melt persisted to low temperature (<300°C), allowing continued small-scale, localized mobilization during late deformation. Although gold occurs at moderate concentrations within the compressional high-strain domains, it is particularly concentrated in the dilational domains, a consequence of its mobilization within a sulfosalt melt. Our model of partial melting of the ore mineral assemblage with consequent mobilization explains how ore minerals that are unstable even at greenschist facies conditions came to be hosted in structures that formed at or near the peak of amphibolite facies metamorphism.

Introduction

Melting of sulfide mineral assemblages during metamorphism of a preexisting mineral deposit has been recognized at a small number of localities (e.g., Hofmann, 1994; Mavrogenes et al., 2001; Tomkins and Mavrogenes, 2002). However, it is likely that sulfide melting has gone unrecognized at many other previously described mineral deposits (Frost et al., 2002). This is likely due to the difficulty in recognizing textures that can be unequivocally related to sulfide melt, and a general lack of awareness that ore mineral assemblages can melt during metamorphism.

Recognition of sulfide melting is important because there are several implications for mine exploitation, as well as local and possibly regional exploration. For example, sulfide melts are highly mobile, with viscosities close to that of water (e.g., Dobson et al., 2000), and thus migrate easily (Tomkins and Mavrogenes, 2002), enabling melt accumulation in structurally favorable sites. These sites could potentially be located significant distances (possibly kilometers) away from where the melts were originally generated. In addition, sulfide melts strongly partition precious metals such as gold and silver (Mavrogenes et al., 2001; Frost et al., 2002; Tomkins and Mavrogenes, 2002), thus potentially leading to the formation of precious-metal–rich segregations and, perhaps, precious-metal halos or caps around the main sulfide orebody.

In this study, we examine the Hemlo gold deposit, which Frost et al. (2002), in a global review of sulfide melting during metamorphism, considered likely to have experienced sulfide melting during middle to upper amphibolite facies metamorphism. Hemlo, in central Ontario, Canada (Fig. 1), is currently Canada's third-largest lode gold deposit (95 Mt at 8.0 g/t; Schnieders et al., 2000). Much of the research on Hemlo has focused on the timing of mineralization, relative to amphibolite facies metamorphism. Most early studies favored a postpeak metamorphic timing (Hugon, 1986; Masliwec et al., 1986; Walford et al., 1986; Hattori, 1987; Corfu and Muir, 1989; Johnston and Smyk, 1992; Pan and Fleet, 1992), although others supported a pre- or synmetamorphic timing (Cameron and Hattori, 1985; Goldie, 1985; Kuhns, 1986, 1988; Valliant and Bradbrook, 1986; Thode et al., 1991). In the mid-1990s, Kuhns et al. (1994), Gustafson (1995), and Michibayashi (1995) supported a premetamorphic timing,

† Corresponding author: e-mail, atomkins@ucalgary.ca

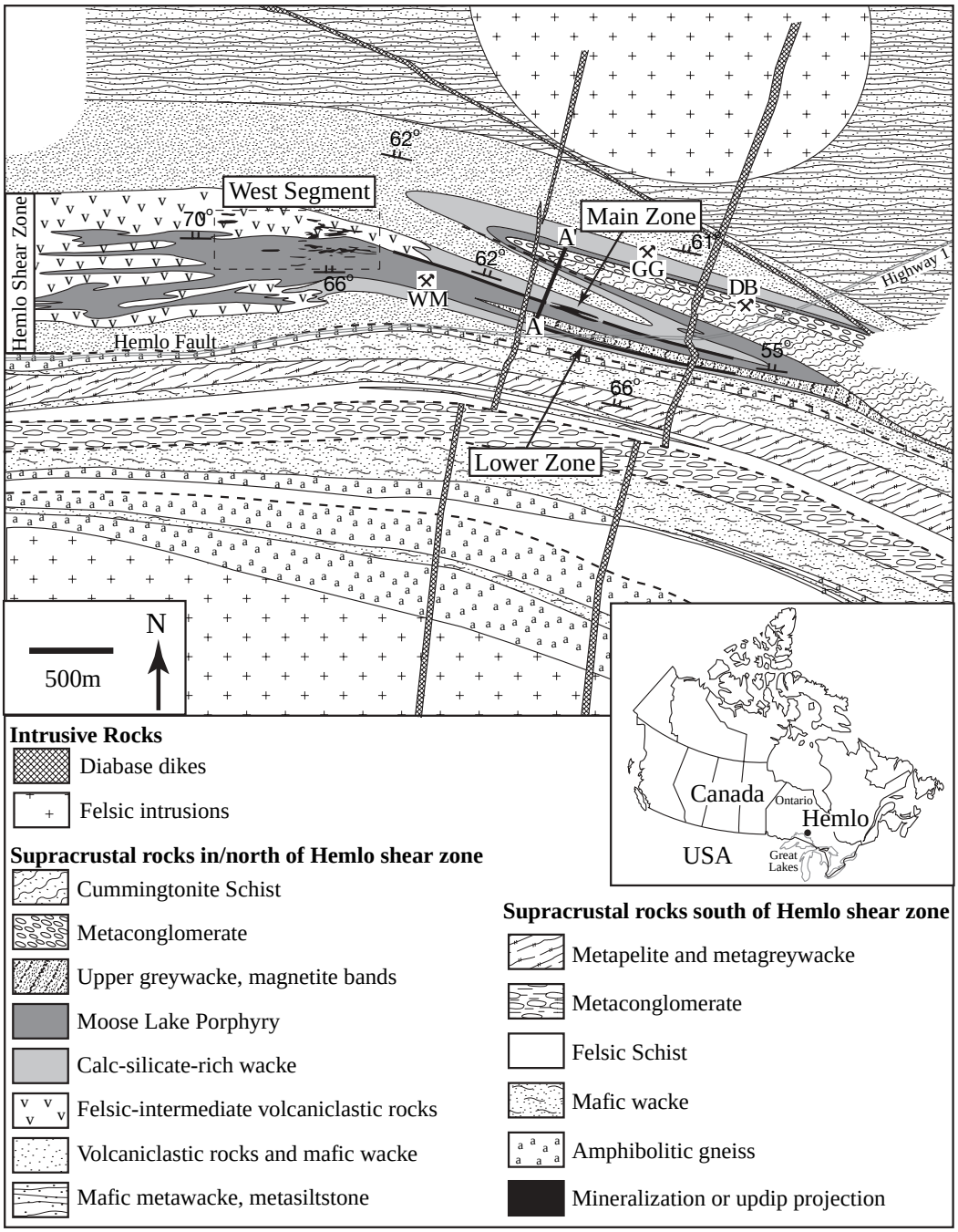

FIG. 1. Location of the Hemlo gold deposit and geologic map of the area around the deposit (simplified from Lin, 2001). Figure 2 is a section at A-A'. DB = David Bell mine, GG = Golden Giant mine, WM = Williams mine.

and Fleet and Pan (1995) and Pan and Fleet (1995) supported a postmetamorphic timing. Since then, all authors have favored a pre- to synpeak metamorphic timing for the mineralization (Johnston, 1996; Powell and Pattison, 1997; Powell et al., 1999; Bodycomb et al., 2000; Lin, 2001; Muir, 2002, Davis and Lin, 2003, Muir, 2003).

One of the main problems for a pre- or synpeak metamorphic timing is the occurrence of low- to moderate-temperature sulfide minerals (minerals stable only below 350°–600°C) in middle amphibolite-grade host rocks. Several authors have noted that many of the ore minerals are not stable at these conditions, and consequently concluded that crystallization of these minerals must have postdated peak metamorphism (e.g., Burk et al., 1986; Harris, 1989). Powell and Pattison (1997) suggested that these minerals exsolved from a complex solid solution at peak metamorphic conditions. However, these authors did not consider the melting temperatures of the solid solutions and, more importantly, the melting relations between coexisting sulfide phases. Another enigmatic aspect of the Hemlo deposit is the heterogeneous

distribution of ore minerals in relation to meso- and microstructural domains. Although much of the sulfide material in the deposit is situated in highly strained rocks, a significant volume of low- to moderate-temperature sulfosalts, as well as gold, is hosted in ductile structures formed at high temperature (e.g., Bodycomb et al., 2000). These structural features formed approximately concurrently with peak metamorphism and continued to be reactivated during postmetamorphic ductile deformation (Lin, 2001).

The primary aim of this paper is to examine the hypothesis that the ore mineral assemblage underwent partial melting during concurrent metamorphism and deformation, leading to mobilization of the melt. We first describe the ore assemblages and their distribution with respect to various meso- and microstructural domains within the deposit, and briefly discuss possible mobilization mechanisms. We then review experimentally determined phase relations between the relevant minerals, which show that melting was inevitable and that melting of some phases and lack of melting of others can explain the observed heterogeneity in ore mineral distribution within the deposit. The significance of our results to mine exploitation and exploration strategies is also discussed.

Geology of the Hemlo Gold Deposit

The general geology of the Hemlo gold deposit has been described in numerous papers (see Muir, 2002, for a detailed review). Only details relevant to this paper are included here. Hemlo is an Archean gold deposit, situated in the Hemlo-Schreiber greenstone belt of the Superior province (Wawa subprovince), northwestern Ontario. Williams et al. (1991) presented an overview of the regional geology of the Wawa subprovince, including the Hemlo-Schreiber greenstone belt. Hemlo is located within a zone of strong deformation, known locally as the Hemlo shear zone, which parallels the regional west-northwest structural trend.

The deposit is situated within a broad zone of metamorphosed alteration that is up to 400-m wide and more than 4-km long. The mineralization is divided into two segments known as the Main and West segments (Muir, 2002). Although both segments dip ~60° to the north, the Main Segment strikes at ~290° and the West Segment strikes at ~270° (Fig. 1). Both segments consist of zones of tabular, shear-zone–parallel mineralization. The Main Segment contains an upper Main Mineralized zone and a smaller, subparallel Lower Mineralized zone (Fig. 2), and the West Segment comprises a series of narrow, erratically mineralized, low-grade zones.

A range of rock types hosts mineralization, including metasedimentary rocks, quartz feldspar porphyry, baritic metasediments, and a mafic fragmental unit (possibly volcaniclastic; Bodycomb et al., 2000). Barite is a major constituent of the deposit (Harris, 1989). These lithologies are affected by pervasive, prepeak metamorphic alteration that varies across the deposit, locally overprinted by (syn- to postpeak metamorphic?) fracture- and/or cleavage-controlled alteration (Muir, 2002). The premetamorphic alteration is thought to represent primary alteration associated with the original mineralization event (A.E. Williams-Jones, unpub. report for the Canadian Mineral Industry Research Organization, 1998). In general,

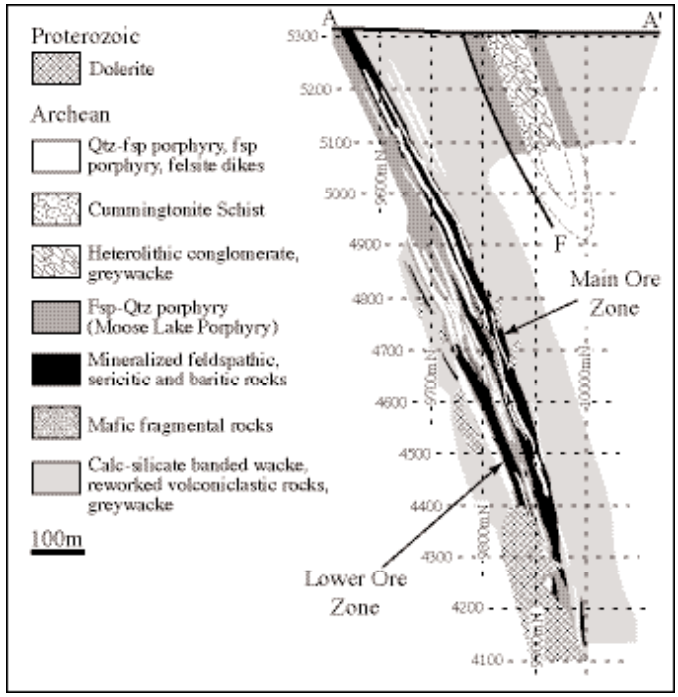

FIG. 2. Geologic section through the Main Segment of the Hemlo orebody (along A-A' from Fig. 1, at 10,000 east, Golden Giant mine), showing the Main and Lower Ore zones (modified from a section provided by Golden Giant mine). Fsp = feldspar, qtz = quartz.

pervasive alteration is narrower in the Main Segment than in the West Segment, a pattern followed by mineralization, which is also narrower and of a higher grade in the east. Pervasive alteration is characterized by enrichment in K, Au, Mo, Sb, As, Hg, Ba, and V, and depletion in Na, Ca, Mg, and Mn (Kuhns, 1986); although some parts, particularly in the West Segment, are characterized by enrichment in Na or Si and depletion in K (Muir, 1997). Mineralogically, the pervasive alteration is characterized by a central zone of K-feldspar-quartz-(muscovite-biotite) rocks surrounded by muscovite-quartz schists (A.E. Williams-Jones, unpub. report for the Canadian Mineral Industry Research Organization, 1998). Silicification, biotitization, and pyritization are thought to be important components of the potassic alteration. Mafic fragmental rocks in the ore zone typically display extensive biotitic alteration, which is locally overprinted by muscovitic alteration. Muir (2002) notes four types of fracture-controlled alteration, which include, in order of abundance, the following: feldspar, biotite, pyrite + feldspar, and carbonate. These occur independently of mineralization, although pyrite + feldspar alteration typically involves enrichment in Au, Ba, Hg, and Mo within mineralized zones.

Five periods of deformation are thought to have affected the host rocks at the Hemlo deposit (Lin, 2001; Muir, 2002). D_1 is recorded by locally preserved isoclinal folds, sheath folds, and fault zones (Muir, 2002), although it may be related to a single period of deformation that progressed into D_2 (Lin, 2001; Muir, 2002). D_2 was the dominant deformation event at Hemlo and is associated with development of the Hemlo shear zone, as well as tight to isoclinal folding. Ductile

deformation during D_2 induced a degree of structural heterogeneity within the deposit, which is preserved as a series of micro- to mesoscale (100-μm to 1.5-m) dilational domains within moderately to highly strained rock. These low-strain, dilatant domains are a consequence of competency contrasts that developed between relatively incompetent mica-rich rocks and relatively competent mica-poor rocks. The competent layers and veins were boudinaged and experienced extensional fracturing, producing dilational areas at the boudin necks and fractures. Fold hinges and pressure shadows behind isolated knots of competent material are other examples of dilational domains that formed in and around more competent units. These features are best preserved in quartz veins, many of which were so strongly folded and boudinaged by this event that they were dismembered into isolated quartz knots. In a period of northwest-directed transpression (Muir, 2003), D_3 produced open to tight, z-shaped folds (indicating dextral shear), many of which are spatially associated with previously boudinaged feldspar porphyry dikes (Lin, 2001). The D_2 dilational features were locally enhanced during D_3. D_4 and D_5 were minor, late events that produced kink bands and brittle faults, respectively.

The host rocks are interpreted to have experienced a single cycle of metamorphism, which peaked at 600° to 650°C and 6 to 7 kbars, and followed a clockwise P-T path (Powell et al., 1999). Based on the relationships of kyanite and sillimanite to fabrics and microstructures (Powell et al., 1999), peak metamorphism is interpreted to have been reached during D_2, with isothermal decompression commencing in the waning stages of D_2. The continued production of ductile structures during D_3 indicates that high temperatures prevailed during this event. The most recent interpretations of the timing of mineralization with respect to deformation indicate that ore emplacement occurred prior to or during the initial stages of D_2 (Lin, 2001; Davis and Lin, 2003), or possibly during middle D_2 (Muir, 2002; Muir, 2003). Davis and Lin (2003) have bracketed the age of mineralization between 2685 ± 4 Ma and 2677 ± 1 Ma.

Description and Distribution of the Ore Assemblages

More than 50 ore minerals at Hemlo fit into four general categories (Harris, 1989; Table 1): (1) common sulfides and sulfosalts, (2) Tl-Pb-Cu-Hg-Ag–bearing sulfosalts, (3) native metals and intermetallic compounds, and (4) tellurides and selenides. In this paper, we refer to stibnite (Sb_2S_3), realgar (AsS), and orpiment (As_2S_3) as sulfosalts (strictly, a sulfosalt is a mineral with metal(s), metaloid(s), and sulfur), because As and Sb are metaloids, and this chemical distinction allows us to differentiate between melting of sulfosalts and metallic sulfides, which melt at generally higher temperatures. The ore minerals are heterogeneously distributed with respect to meso- and microstructural domains throughout the deposit (Table 1). We have divided the ore mineral suite into two groups, based on structural association. Group I minerals are typically disseminated within higher strain, mica- and K-feldspar–rich domains, and include pyrite, molybdenite, pyrrhotite, sphalerite, and cinnabar. This group makes up the majority of sulfide material in the deposit, with pyrite and molybdenite accounting for >95 percent of the total sulfide volume. Group II minerals are volumetrically dominated by stibnite and realgar and comprise an array of rare sulfosalts, tellurides, and native minerals, including gold. These are preferentially concentrated in low-strain, structurally dilatant domains, and many rarely, if ever, occur in high-strain domains. Group I minerals also occur in low-strain, dilatant domains, although they are typically not more concentrated there than elsewhere. However, we have observed rare instances where sphalerite and/or pyrrhotite are concentrated in dilational domains. Some minerals, including gold, are commonly observed in both structural domain types and thus have been included in both groups. Others (e.g., Bodycomb et al., 2000) have similarly noted a heterogeneous ore mineral distribution. Group I minerals compose roughly 5 to 20 percent of the bulk rock volume (locally exceeding 50%), whereas Group II minerals make up <2 percent. Figure 3 illustrates schematically the distribution of Group I relative to Group II minerals at Hemlo.

Mineralization in higher strain compressional domains

Figure 4A and B shows examples of mineralization in high-strain compressional domains. The most common of these is banded pyrite, which consists of pyrite and silicate minerals, although minor pyrrhotite is present at some localities. Pyrite + molybdenite mineralization is also widespread within high-strain compressional domains. In many samples, the highly ductile nature of molybdenite has focused deformation such that the most molybdenite rich regions are typically the most highly strained. Sphalerite and cinnabar also occur in high-strain compressional regions. Harris (1989) noted that minor chalcopyrite and galena occur in some sphalerite-pyrite–bearing samples.

Figure 4C shows a typical example of K-feldspar–rich rock with abundant disseminated pyrite and minor molybdenite,

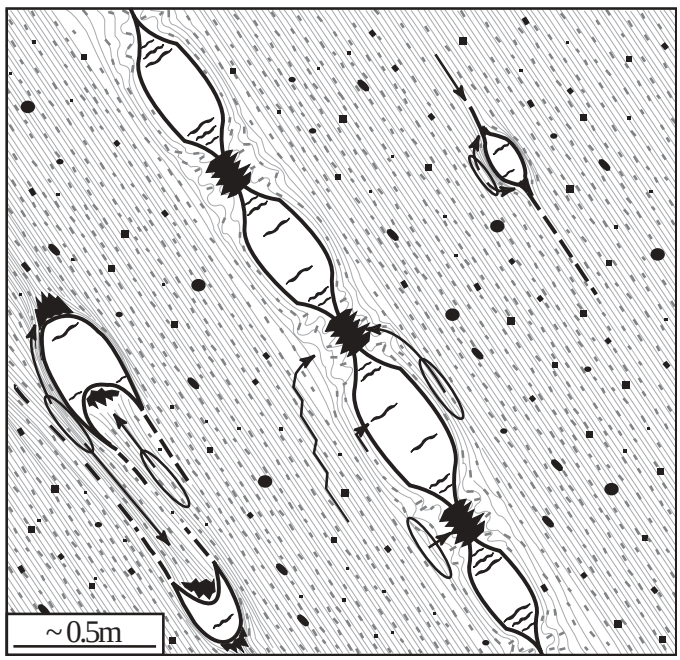

FIG. 3. Schematic diagram illustrating the relative distribution of group I minerals (disseminated gray and black specks) and group II minerals (black shading at boudin necks and in extensional fractures). Arrows indicate melt migration pathways.

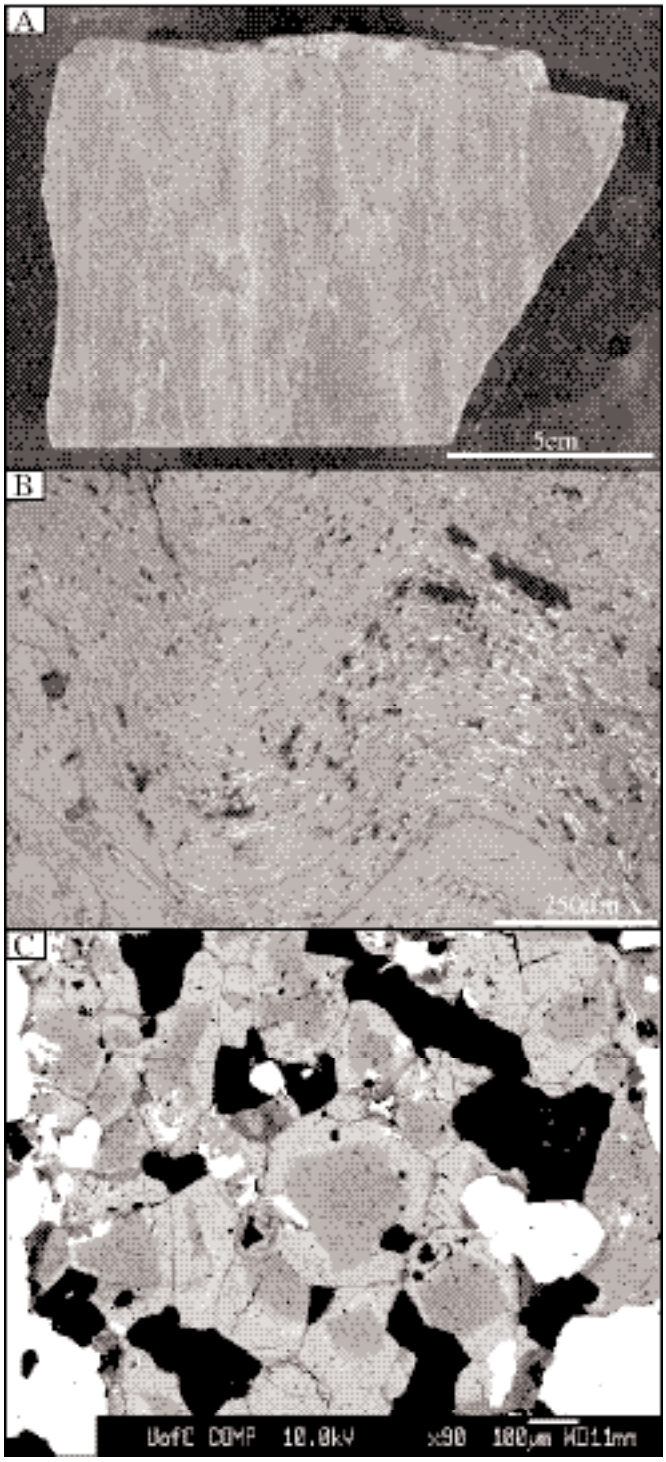

FIG. 4. Examples of mineralization in compressional domains. A. Banded pyrite-molybdenite ore. Fine-grained molybdenite gives the rock a smoky gray appearance. B. Photomicrograph of molybdenite-rich ore (reflected light). In this sample, the preferred orientation of molybdenite (white) defines the D_2 fabric, which is folded by D_3. Gold in this type of ore rarely exceeds 20 μm in longest dimension. C. Back-scattered electron image of K-feldspar–quartz rock. The zoned grains are microcline with Ba zoning (brighter zones reflect higher Ba). The black areas are quartz, and the white areas are pyrite and barite.

which is widespread at Hemlo (contrast has been adjusted to highlight Ba zoning in the K-feldspar). The granoblastic nature of this rock indicates lower strain than in the examples shown in Figure 4A and B. If layers such as this are part of a relatively undeformed thick sequence with little ductile material (mica and molybdenite), they are still considered compressional when compared with actively dilational structures. However, if two mica-rich layers occur on either side, this layer would typically be boudinaged, with dilational domains developed at the boudin necks.

Mineralization in dilational domains

Figure 5 shows the relationship between mineralization in compressional and dilational domains within the Main Ore zone. Although a wide range of ore minerals is situated in structurally dilatant sites, stibnite and realgar make up the bulk of the sulfide volume. At the mesoscopic scale, Group II minerals are concentrated at boudin necks in deformed, competent lithologies (Figs. 5 and 6A). At the microscopic scale, they (particularly realgar) are also distributed along a myriad of interconnected fractures within the competent unit (Figs. 5 and 6B). It is common for a large clot of stibnite and/or realgar to contain an array of rare Group II minerals along the periphery of the clot (Fig. 6C), a feature that is mirrored by smaller clots of other Group II minerals (Fig. 7). These large clots of stibnite ± realgar are typically central to an array of fractures (Fig. 6B) that are partially filled with less-common Group II minerals. Fractures are typically the sites that contain gold and the other native metals and intermetallic compounds (Fig. 6D), although they also occur along grain boundaries between coarse stibnite and realgar (Fig. 5). Many large clots of stibnite contain exsolution lamellae, usually of realgar, but also of some of the rare sulfosalts (Fig. 6E). Most stibnite analyses show that some As substitution for Sb is preserved (Table 1), and thus that the exsolution process is incomplete. Powell and Pattison (1997) also showed examples of rare minerals associated with stibnite and realgar.

Gold mineralogy and distribution

Gold (containing up to 26.9% Hg and 29.1% Ag) occurs in both compressional and dilational domains. The molybdenite-pyrite mineralization typical of higher strain compressional domains makes up the bulk of ore-grade material at Hemlo. However, in this study, gold has been found to be highly concentrated in the low-strain, dilational domains (Fig. 5), even when compared to extremely molybdenite rich samples. A typical bulk ore grade at Hemlo is on the order of 10 ppm Au (avg grade for the deposit is 9.9 ppm Au; Johnston, 1996), but we have observed several examples of dilational domains that contain well in excess of 100 ppm Au. In compressional regions, gold is typically sparse and very fine grained (<20 μm), whereas gold in dilational domains is both more abundant and coarser grained (up to 1 mm). Gold grains in dilational sites are commonly rimmed by native arsenic (Fig. 7A) and/or aurostibite ($AuSb_2$; Fig. 7B, C), and have grain boundary contacts with many of the Group II minerals (examples are shown in Figs. 5 and 6). Hg and Ag are uniformly distributed in some gold grains and zoned in others, the zonation showing a relationship with adjacent

TABLE 1. Ore Minerals Identified in the Hemlo Deposit: Their Compositions and Structural Associations

Mineral	Formula	Hemlo details	Typical structural position	Mineral group	Abundance	Reference
Common sulfides and sulfosalts						
Pyrite	FeS_2		High-strain zones[1]	Group I	Very common	Harris (1989)
Molybdenite	MoS_2		High-strain zones[1]	Group I	Very common	Harris (1989)
Sphalerite	ZnS	0–29.5% Hg; 0–1.9% Fe; 0–6% Mn	High-strain zones[1]	Group I	Common	Harris (1989), this study
Stibnite	Sb_2S_3	0–4.8% As	Low-strain, dilational zones[1]	Group II	Common	Harris (1989)
Realgar	AsS	0–0.5% Sb	Low-strain, dilational zones[1]	Group II	Common	Harris (1989)
Cinnabar	HgS		High- and low-strain zones[1]	Groups I and II	Common	Harris (1989)
Tetrahedrite	$(Cu,Ag,Hg)_{10}(Fe,Zn,Cu,Hg)_2Sb_4S_{13}$	0–19% Hg; 0–9% Ag; 0–8% Fe; 0–7% Zn	Low-strain, dilational zones[1]	Group II	Common	Harris (1989), this study
Tennantite	$(Cu,Ag,Hg)_{10}(Fe,Zn,Cu,Hg)_2As_4S_{13}$	0–15% Hg; 0–8% Ag; 0–6% Fe; 0–8% Zn	Low-strain, dilational zones[1]	Group II	Common	Harris (1989), this study
Pyrrhotite	$Fe_{(1-x)}S$		High-strain zones[1]	Group I	Variable	Harris (1989)
Arsenopyrite	FeAsS		High- and low-strain zones[1]	Groups I and II	Variable	Harris (1989)
Orpiment	As_2S_3	0–5.0% Sb	Low-strain, dilational zones[1]	Group I	Uncommon	Harris (1989)
Chalcopyrite	$CuFeS_2$		High-strain zones[2]	Group I	Uncommon	Harris (1989)
Galena	PbS		High-strain zones[2]	Group I	Uncommon	Harris (1989)
Gersdorfite	NiAsS	1.4–14.9% Fe	High-strain zones[2]	Group I	Uncommon	Harris (1989)
Cubanite	$CuFe_2S_3$		High-strain zones[2]	Group I	Uncommon	Harris (1989)
Tl-Pb-Hg-Cu-Ag–bearing sulfosalts						
Zinkenite	$Pb_9Sb_{22}S_{42}$	0–11.5% As	Low-strain, dilational zones[1]	Group II	Uncommon	Harris (1989)
Twinnite	$Pb(Sb,As)_2S_4$	$Pb(Sb_{1.2}As_{0.8})S_4$	Low-strain, dilational zones[1]	Group II	Uncommon	Harris (1989)
Aktashite	$Cu_6Hg_3As_4S_{12}$	$Cu_6Hg_3(As,Sb)_4S_{12}$	Low-strain, dilational zones[1]	Group II	Uncommon	Harris (1989)
Berthierite	$FeSb_2S_4$	Mn: 0–13.4%	Low-strain, dilational zones[1]	Group II	Rare	Harris (1989)
Geochronite	$Pb_{14}(Sb,As)_6S_{23}$	$Pb_{14}(Sb_{3.0}As_{3.0})S_{23}$	Low-strain, dilational zones[2]	Group II	Rare	Harris (1989)
Gudmundite	FeSbS		Low-strain, dilational zones[2]	Group II	Rare	Harris (1989)
Boulangerite	$Pb_5Sb_4S_{11}$	2.4–5.8% As	Low-strain, dilational zones[1]	Group II	Rare	Harris (1989)
Bournonite	$PbCuSbS_3$	0–6.0% As	Low-strain, dilational zones[1]	Group II	Rare	Harris (1989)
Routhierite	$TlCu(Hg,Zn)_2(As,Sb)_2S_3$	$TlCuHg_2(As_{1.4}Sb_{0.6})S_6$	Low-strain, dilational zones[1]	Group II	Rare	Harris (1989)
Parapierrotite	$Tl(Sb,As)_5S_8$	$TlSb_5S_8$	Low-strain, dilational zones[1]	Group II	Rare	Harris (1989)
Chalcostibite	$CuSbS_2$		Low-strain, dilational zones[1]	Group II	Rare	Harris (1989)
Baumhauerite	$Pb_3As_4S_9$	$Pb_3As_{2.2}Sb_{1.8}S_9$	Low-strain, dilational zones[2]	Group II	Rare	Harris (1989)
Criddleite	$TlAg_2Au_3Sb_{10}S_{10}$		Low-strain, dilational zones[1]	Group II	Rare	Harris (1989)
Jamesonite	$Pb_4FeSb_6S_{14}$		Low-strain, dilational zones[2]	Group II	Rare	Harris (1989)
Tvalchrelidzeite	$Hg_{12}(Sb,As)_8S_{15}$	$Hg_{12}(Sb_{4.7}As_{3.3})S_{15}$	Low-strain, dilational zones[2]	Group II	Rare	Harris (1989)
Ullmanite	NiSbS		Low-strain, dilational zones[2]	Group II	Rare	Harris (1989)
Paakkonenite	Sb_2AsS_2		Low-strain, dilational zones[2]	Group II	Rare	Pan and Fleet (1992)
Vaughanite	$TlHgSb_4S_7$		Low-strain, dilational zones[1]	Group II	Rare	Harris (1989)
Seligmannite	$PbCuAsS_3$	$PbCu(As_{0.52}Sb_{0.48})S_3$	Low-strain, dilational zones[2]	Group II	Rare	Harris (1989)
Dufrenoysite	$Pb_2As_2S_5$	$Pb_2(As_{1.1}Sb_{0.9})S_5$	Low-strain, dilational zones[2]	Group II	Rare	Harris (1989)
Galkhaite	$(Cs,Tl)(Hg,Cu,Zn)_6(As,Sb)_4S_{12}$		Low-strain, dilational zones[2]	Group II	Rare	Harris (1989)
Hutchisonite	$(Pb,Tl)_2(As)_5S_9$	$(Pb,Tl)_2(As,Sb)_5S_9$	Low-strain, dilational zones[1]	Group II	Rare	This study
Chabourneite	$(Tl,Pb)_{21}(Sb,As)_{91}S_{147}$	$(Pb,Tl)_{21}(As,Sb)_{91}S_{147}$	Low-strain, dilational zones[1]	Group II	Rare	This study
Rathite	$(Pb,Tl)_3(As)_5S_{10}$	$(Pb,Tl)_3(As,Sb)_5S_{10}$	Low-strain, dilational zones[1]	Group II	Rare	This study
Unknown phase	$AgFeS_2$		Low-strain, dilational zones[2]	Group II	Rare	Pan and Fleet (1992)
Unknown phase	$Pb_2Tl_5(Sb,As)_{24}S_{43}$		Low-strain, dilational zones[2]	Group II	Rare	Harris (1989)
Native metals and intermetallic compounds						
Gold	Au	Up to 26.9% Hg and 29.1% Ag	Concentrated in dilational zones[1]	Groups I and II	Uncommon	Harris (1989), this study
Arsenic	As		Low-strain, dilational zones[1]	Group II	Uncommon	Harris (1989)
Antimony	Sb	0–1.3% As	Low-strain, dilational zones[1]	Group II	Rare	Harris (1989)
Aurostibite	$AuSb_2$		Low-strain, dilational zones[1]	Group II	Rare	Harris (1989)

TABLE 1. *(Cont.)*

Mineral	Formula	Hemlo details	Typical structural position	Mineral group	Abundance	Reference
Stibarsen	SbAs		Low-strain, dilational zones[1]	Group II	Rare	Harris (1989)
Silver	Ag		Low-strain, dilational zones[2]	Group II	Rare	Harris (1989)
Breithauptite	NiSb		Low-strain, dilational zones[2]	Group II	Rare	Harris (1989)
Tellurides and selenides						
Coloradoite	HgTe		Low-strain, dilational zones[1]	Group II	Rare	Harris (1989)
Calaverite	AuTe2		Low-strain, dilational zones[1]	Group II	Rare	Harris (1989)
Petzite	Ag_3AuTe_2		Low-strain, dilational zones[1]	Group II	Rare	Pan and Fleet (1992)
Hessite	Ag_2Te		Low-strain, dilational zones[1]	Group II	Rare	Pan and Fleet (1992)
Melonite	$NiTe_2$		Low-strain, dilational zones[2]	Group II	Rare	Harris (1989)
Altaite	PbTe		Low-strain, dilational zones[2]	Group II	Rare	Harris (1989)
Unknown phase	$AgSbTe_2$		Low-strain, dilational zones[2]	Group II	Rare	Harris (1989)
Clausthalite	PbSe		Low-strain, dilational zones[2]	Group II	Rare	Harris (1989)

Notes: Where possible, minerals are listed approximately in order of abundance for each category; in the reference column we have only referred to this study where we have added to the published information; minerals in this study were identified by electron microprobe

[1] The association was observed in this study

[2] An inferred structural position based on information in Harris (1989), or on composition and mineral associations

sulfides. For example, in Figure 7D a gold grain with relatively Ag and Hg rich margins abuts stibnite, and the zoning is absent adjacent to the stibnite. Aurostibite is commonly associated with gold and native stibnite, as well as with the gold-bearing Tl-sulfosalt, criddleite ($TlAg_2Au_3Sb_{10}S_{10}$; Harris, 1989). Calaverite ($AuTe_2$) and petzite (Ag_3AuTe_2) are associated with the other tellurides, as well as with native arsenic, tennantite, realgar, and gold (Harris, 1989).

Evaluation of Alternative Mobilization Mechanisms

There are three different mechanisms that may have concentrated precious metals and sulfosalts in dilational structures at Hemlo: solid-state mobilization, dissolution and/or reprecipitation associated with a hydrothermal fluid, or migration of polymetallic melt. In fact, it is likely that all three of these were responsible for some degree of mobilization at Hemlo, although we aim to show that the latter was the dominant mechanism.

Deformation during and after peak metamorphism is expected to have been the driving force for mobilization of precious metals and sulfosalts at Hemlo. In any deforming multiphase medium, some phases deform more easily (are less competent) than others. These mobile phases move down hydraulic gradients that develop between compressional and dilational regions during deformation, to collect in dilational sites. Various authors have noted that many sulfides undergo solid-state mobilization through this process, because they become ductile at lower temperatures than do silicates and so are preferentially transported (see Marshall et al., 2000, for a comprehensive review). Molybdenite is particularly ductile, yet apart from localized concentrations at meso- to microscale fold hinges, there is no evidence for preferential concentration of molybdenite in dilational sites. In fact, because of strain partitioning, molybdenite-rich regions are generally the most highly strained, and molybdenite is abundant in high-strain compressional domains. Some of the other Group I minerals (e.g., pyrrhotite and sphalerite) are also known to be ductile at 600°C, but they only rarely occur in dilational sites. These observations suggest that solid-state mobilization was not responsible for the majority of the sulfide redistribution.

During prograde metamorphism, rocks that contain hydrous minerals undergo a range of metamorphic dehydration reactions. Thus, during peak metamorphism at Hemlo, there would have been some hydrothermal fluid moving through the rock with the capacity to dissolve sulfides and other metallic minerals and mobilize their constituent elements. During deformation, this hydrothermal fluid would be preferentially focused into dilational domains through the same mechanism discussed above. As is shown below, most of the Group II minerals now observed in dilational sites are not stable at peak metamorphic conditions (some assemblages are only stable at very low temperatures of <300°C). Therefore, if hydrothermal mobilization were responsible for the majority of metal redistribution and led to precipitation of the observed sulfosalt mineral suite, it must have taken place after significant cooling from peak metamorphic temperatures. However, not only is there typically little water available during the retrograde portion of metamorphic cycles, the dilational structures where the minerals are located are syn- to late-peak ductile structures (D_2 and D_3) that were

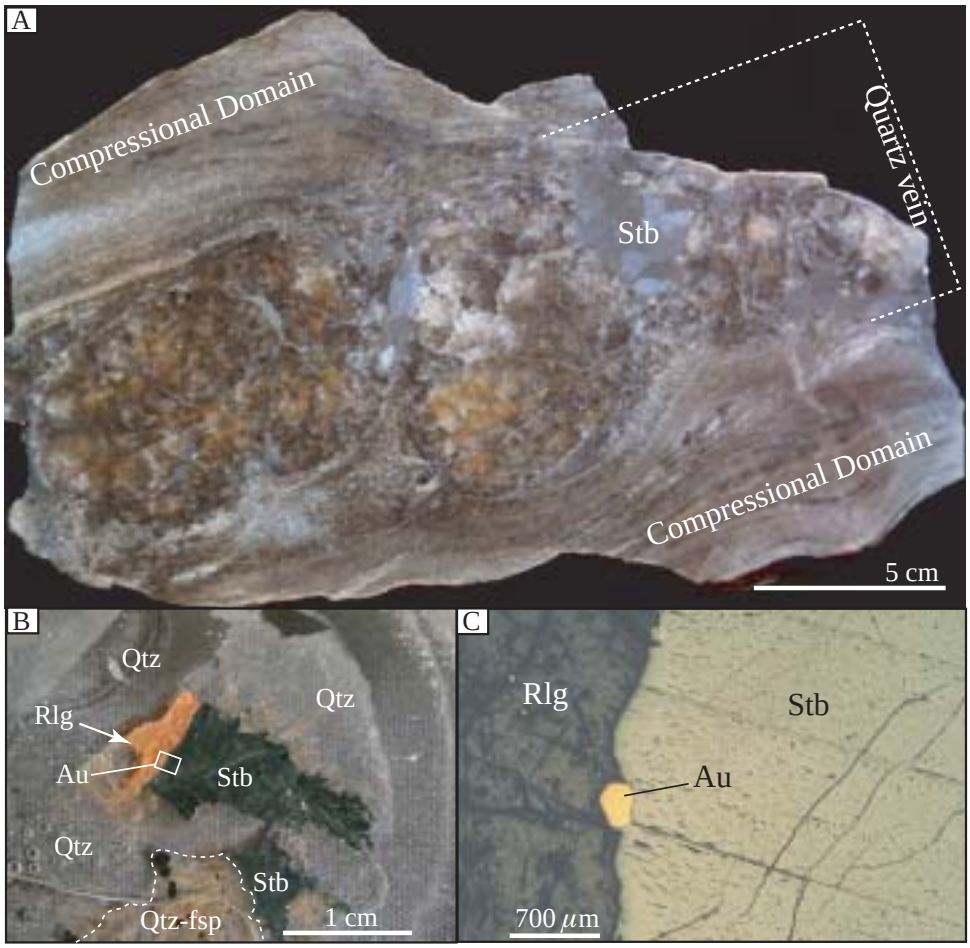

FIG. 5. Photographs highlighting the contrasts between mineralization in compressional and dilational domains. A. An example of a strongly boudinaged quartz vein with coarse clots of sulfosalts (dominated by stibnite—Stb) concentrated at boudin necks and in extensional fractures. The orange coloration in the quartz is produced by realgar that coats a myriad of fine fractures. Note that this is a high-temperature ductile structural feature (probably D_2) that formed approximately concurrently with peak metamorphism B, C. Sulfosalt mineralogy at a boudin-neck accumulation; the area of (C) shows as a small rectangle on (B); fsp = feldspar, Qtz = quartz, Rlg = realgar. Although there is abundant, coarse (up to 1-mm) visible gold in this sample, there is very little in molybdenite-rich compressional domain samples from the immediate vicinity (only rare grains that were <20 μm were found). Sulfides in the nearby compressional domains are dominated by pyrite and molybdenite, whereas in the dilational domains, stibnite and realgar predominate. A range of rare sulfosalts, native metals, and tellurides were also found in the latter. The implications of coexisting stibnite and realgar in (C) are illustrated in Figure 8A and B.

probably inactive at lower temperatures. Only brittle deformation can proceed at the low temperatures required.

The presence of large amounts of sulfosalt in numerous, relatively small dilational domains would have required large volumes of mobilizing fluids (large fluid/rock ratios) well after peak metamorphism. Although some authors have reported localized silicate alteration associated with retrograde hydrothermal mobilization (e.g., Muir, 2002), the intensity and extent of alteration is less than would be expected to account for the volume of fluid required. At some localities, there is no retrograde alteration assemblage at all (Bodycomb et al., 2000), and relatively high temperature metamorphic phases (e.g., feldspar, kyanite, sillimanite) are closely associated with the mobilized ore minerals. Large amounts of hydrothermal fluid at 300°C or less would have completely destroyed these silicate minerals and would have led to sericite-chlorite-clay assemblages. The paucity of postmetamorphic quartz-carbonate veins associated with mobilized mineralization also argues against a major role for hydrothermal fluids.

In addition, Wood et al. (1987) conducted a series of solubility experiments on the assemblage, pyrite-pyrrhotite-magnetite-sphalerite-galena-gold-stibnite-bismuthinite-argentite-molybdenite, with H_2O-NaCl-CO_2 solutions from 200° to 350°C. They found that in chloride-free solutions, the relative solubilities follow the sequence Sb > Fe > Zn > Pb > Ag-Mo > Au-Bi. Fe, Sb, and Zn would, therefore, be preferentially mobilized relative to the other elements in a retrograde environment. Although Sb has been extensively mobilized at Hemlo, neither Fe nor Zn is enriched in most dilational sites, whereas Au, Ag, and Pb are.

These factors suggest that hydrothermal mobilization of ore minerals, as suggested by Pan and Fleet (1995), was not

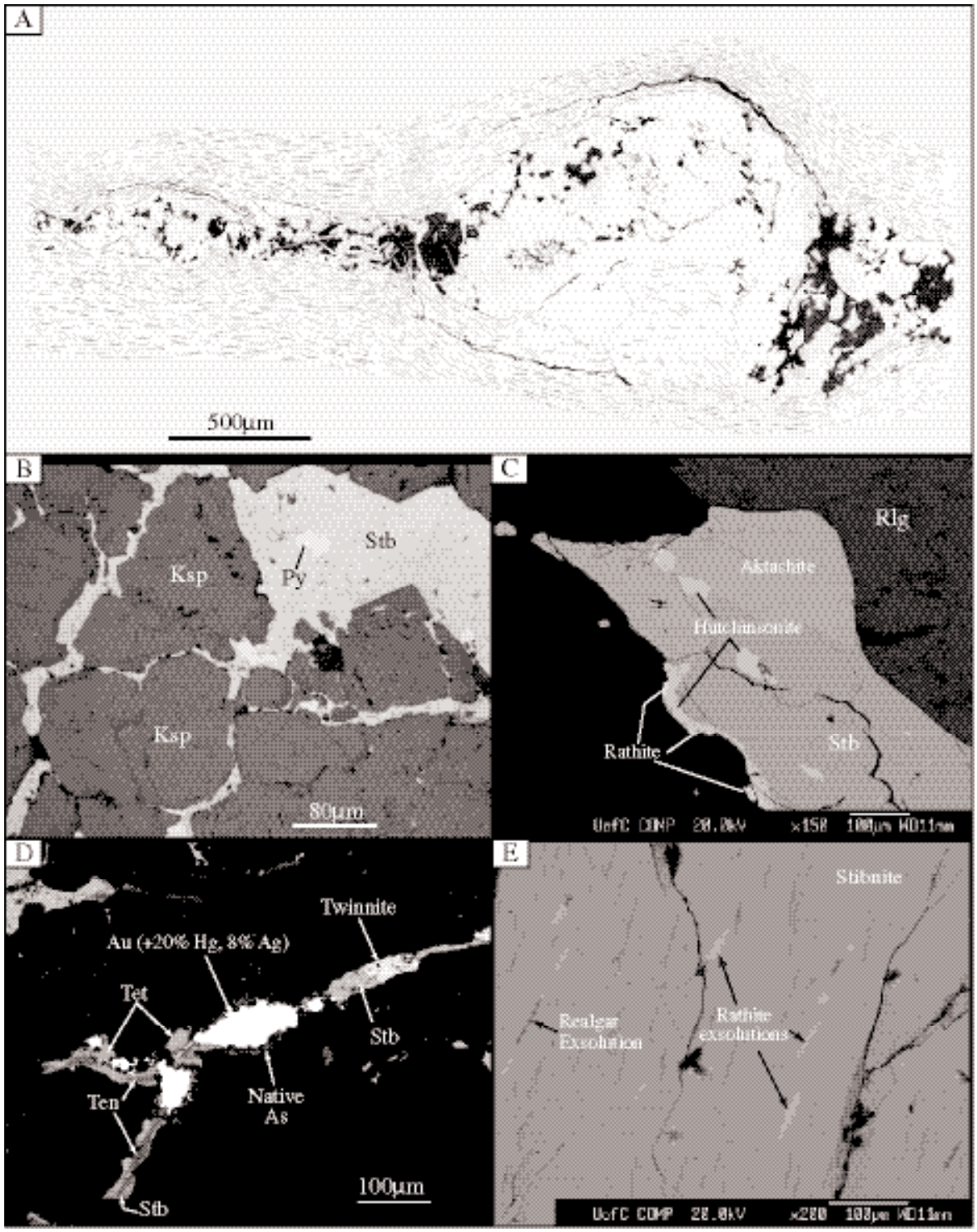

FIG. 6. Examples of mineralization in dilational domains. A. A sketch (from a series of photomicrographs) of a strongly boudinaged feldspar-quartz layer (unfoliated) within muscovitic ore (foliated), showing that stibnite (black) is distributed predominantly at the boudin necks and in extensional fractures in the competent layer. In this sample, disseminated pyrite occurs in the strained muscovite-rich portion and also in the boudinaged layer, but stibnite only occurs within the boudinaged layer and as thin stringers along the high-strain margins. We interpret these thin stringers as migration pathways, where sulfosalt melt migrated before encountering a dilational feature. B. A small accumulation of stibnite (Stb) within a boudinaged K-feldspar–rich layer (Ksp) with radiating fine fractures filled with more stibnite. Elsewhere in this boudinaged layer are additional microfractures filled by realgar and a range of other sulfosalts. C. Edge of the large stibnite-realgar clot in Figure 5 (sample AGT-Hem015e), and an accumulation of the rarer sulfosalts at the periphery. D. Gold in a fracture with native arsenic, tetrahedrite-tennantite (Hg rich), stibnite, and twinnite (sample AGT-Hem003). The composition of the gold in this photomicrograph is plotted in Figure 11C. E. Realgar and rathite exsolutions in stibnite.

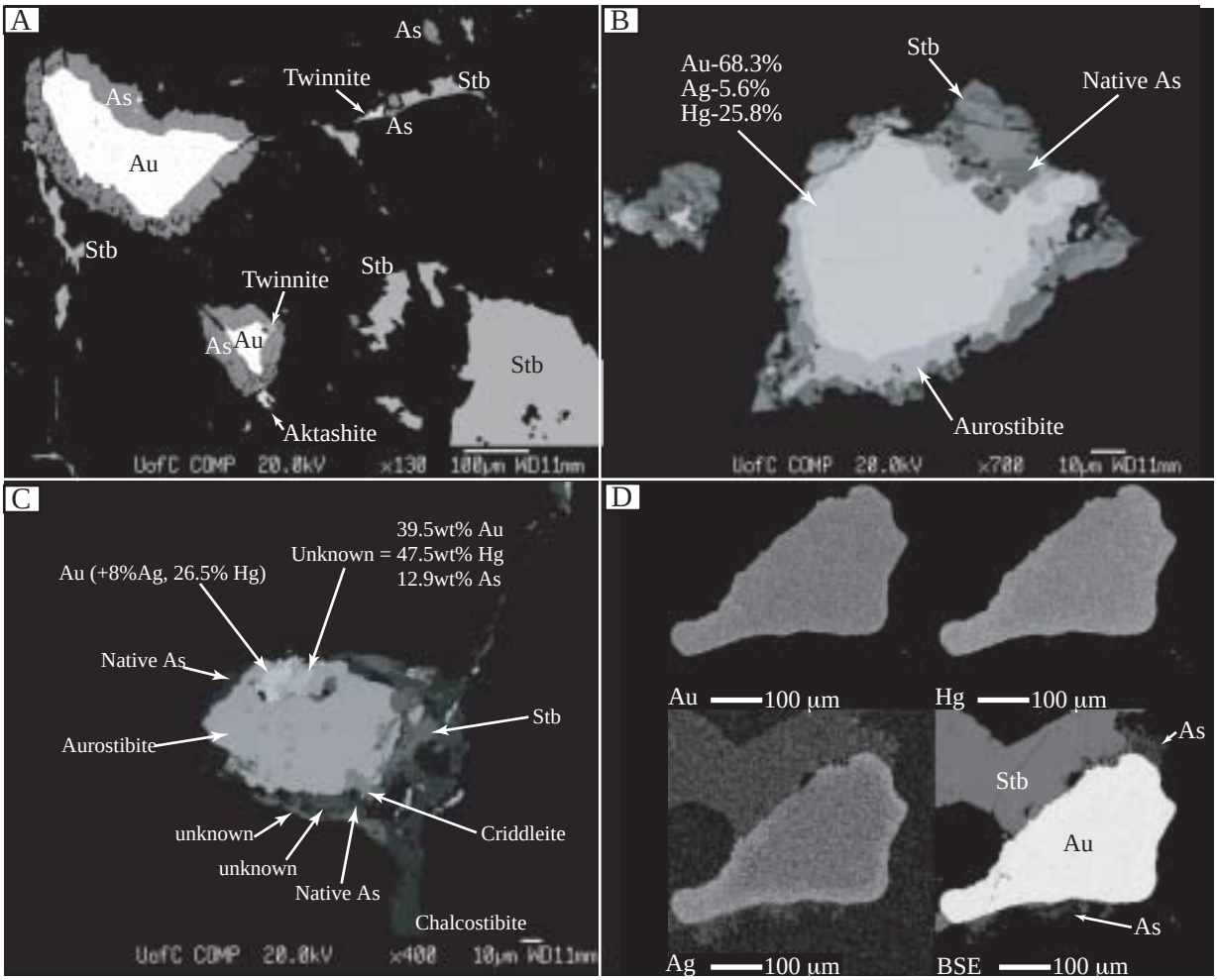

FIG. 7. A. Gold (with Hg and Ag in solid solution) rimmed by native arsenic and in association with stibnite (Stb), twinnite, and aktashite within a fractured quartz boudin. B. Fracture-hosted gold mineral associations within a D_2-boudinaged quartz vein. Gold is rimmed by aurostibite and native arsenic, followed by stibnite. C. More gold mineral associations from the same quartz vein as in (B). In this example, aurostibite is dominant, and many rare and even previously unnamed phases are in close association. The composition of gold in (B) and (C) from sample AGT-Hem004 is highlighted in Figure 11C. Comparison with Figure 11 shows that ore minerals in (B) and (C) must have been molten during peak metamorphism. D. Element maps of a gold grain that abuts stibnite with minor, adjacent native arsenic. It is evident that zonation of Ag and Hg in the gold grain is disturbed where the stibnite abuts.

the major mechanism of remobilization at Hemlo. Therefore, it is possible that the third mechanism, mobilization of a sulfide melt, was responsible for the majority of ore mineral redistribution at Hemlo. Although there have been very few studies on the viscosity of sulfide liquids, it is known that FeS melt has a viscosity similar to that of water at high temperature and pressure (Dobson et al., 2000). This means that sulfide melts would be highly mobile during deformation and would efficiently migrate toward dilational sites from compressional regions. The remainder of the paper examines phase equilibria and textural evidence that supports this hypothesis.

Phase Relations Relevant to the Hemlo Ore Assemblage

At least 15 elements are components of the ore assemblage at Hemlo (Table 1). No single experimental study resolves the complex phase relations involving cotectics, eutectics, and thermal divides in this system. Most published experimental studies are limited to two- to five-component systems. Therefore, we combined the results of these simple, experimentally determined systems to investigate the possible melting behavior of the Hemlo ore assemblage. The selection of elements considered in each subsection is based on actual ore mineral compositions at Hemlo. Unfortunately, there are many gaps in the experimental studies, and the following discussion also highlights areas for further research.

Melting relations among the sulfosalts in the system Sb-As-Tl-Pb-Ag-Cu-Fe-S

Figure 8 contains a series of binary and ternary phase diagrams for subsets of this system. Although there are many possible subsystems for which there are no experimental data (e.g., those involving realgar), it is clear from Figure 8 that, even as isolated phases (not in contact with other minerals),

many of the sulfosalt minerals at Hemlo would be molten at temperatures well below peak metamorphism. For example, orpiment, realgar, and stibnite melt at 310°, 321°, and 556°C, respectively (Fig. 8A and B). Where minerals coexist, a melt is invariably generated at even lower temperatures. Figure 8B and G shows that when stibnite and orpiment (two common phases at Hemlo) coexist, they initially react as temperature increases to form a solid solution ($(Sb,As)_2S_3$). As temperature increases further, this solid solution starts to melt. Figure 8B shows that in this reaction, As-rich local bulk compositions may produce melt at less than 275°C; and by 556°C, even the most Sb-rich solid solution is completely molten. Figure 5B shows coexisting realgar (AsS) and stibnite, which would likely react at similar conditions, given the similar melting points of realgar and orpiment (Fig. 8A). Nearly all stibnite that we examined microscopically had realgar exsolutions, indicating solid solution between these minerals.

By using phase diagrams determined for pure systems (Fig. 8C, D, and I), it is possible to investigate how interaction among stibnite, the arsenic sulfides, and tetrahedrite-tennantite solid solution (tet-ten$_{ss}$), all common at Hemlo, compared to the other sulfosalts (Harris, 1989), would have produced melt if they all existed prior to peak metamorphism. Note that the end members, tetrahedrite ($Cu_{12}Sb_4S_{13}$) and freibergite ($Ag_{12}Sb_4S_{13}$), are considered to be analogous to skinnerite (Cu_3SbS_3; T_m = 610°C) and pyrargyrite (Ag_3SbS_3; T_m = 485°C) in Figure 8C and D, respectively. As an example, when Sb-As-S melt (containing the equivalent of 1 mol of Sb_2S_3) is added to 1 mole of tetrahedrite, without considering the effect of the As, initially the Sb-As-S melt and tetrahedrite would react to form chalcostibite ($CuSbS_2$) and Cu-bearing sulfosalt melt. As temperature increased through ~552°C, the chalcostibite would continue to react with the melt until completely consumed (Fig. 8C). The local bulk composition controls the final melting temperature of all assemblages. If the bulk composition happened to be dominated by tennantite, melting would be complete at ~665°C (Fig. 8I); at slightly lower temperatures, tennantite would only partially melt. Whereas a freibergite-dominated local bulk composition (Fig. 8D) would be completely molten at 485°C. Natural tet-ten$_{ss}$ compositions are likely to melt in a similar fashion, at temperatures somewhere in between. Although the experimental data provide no indication of the effect of Hg substitution on melting of tet-ten$_{ss}$, it is likely that, in the presence of stibnite and/or arsenic sulfides (e.g., Fig. 6D), tet-ten$_{ss}$ would have melted by 600° to 650°C, particularly given that stibnite and As sulfides are significantly more abundant at Hemlo than tet-ten$_{ss}$.

Reaction between stibnite and galena with increasing temperature (Fig. 8E) would initially produce an array of intermediate phases (several of which occur at Hemlo), depending on the local bulk composition, before melting at lower amphibolite facies in stibnite-rich bulk compositions. For example, in a sample containing 5.3 moles of stibnite and 4.7 moles of galena, the initial metamorphic reaction would form zinkenite ($Pb_9Sb_{22}S_{42}$) and robinsonite ($Pb_4Sb_6S_{13}$) at ~330°C. Melting would start at ~546°C, when these react to form robinsonite and Pb-bearing sulfosalt melt. With additional temperature increase, robinsonite would continuously react with the melt until it was completely consumed at ~582°C. Other Pb-Sb sulfosalts found at Hemlo would also start to melt at lower amphibolite facies conditions (Fig. 8H, K, and L). The lowest temperature melts that could theoretically be produced at Hemlo would be those in the system As_2S_3-Sb_2S_3-Tl_2S (Figs. 8G and 6C), in which melting commences at greenschist facies temperatures or lower (<275°C; Sobott, 1984).

Unfortunately, there have been no experimental studies that specifically examine the phase relations between gold and sulfosalts. However, there have been a few studies in which reaction occurred between the sulfosalts and the gold capsules used in the experiments. Clark (1960) noted that arsenopyrite + gold melts at ~670°C, and Roland (1968) found ~2 percent gold by volume in Pb-As-S melts at temperatures as low as 549°C.

By using the binary phase diagrams to examine the tie lines between the ternary end members, we have constructed a composite diagram of ternary sections at 600°C for the system Ag_2S-PbS-Cu_2S-FeS-As_2S_3-Tl_2S-Sb_2S_3 (Fig. 9). This diagram gives a graphic illustration of the extent of melting that would be expected in this system during peak metamorphism at Hemlo. When the bulk sulfosalt assemblage is dominated by stibnite (as observed), all end-member components in this system contribute significantly to a sulfosalt melt, with the exception of FeS (Fig. 8F, H, and J).

Melting of MoS_2, FeS_2, $Fe_{1-x}S$, ZnS, HgS, and MnS, and the effect of solid solutions

Although molybdenite (MoS_2) and pyrite are not known to participate in solid solutions in any system, other phases in the system MoS_2-FeS_2-FeS-ZnS-HgS-MnS form complex solid solutions at high temperatures (Fig. 10). The most extensive solid solution among sulfides observed at Hemlo involves ZnS, FeS, MnS, and HgS (Fig. 10A, B, and C). Figure 10D shows exsolution textures between cinnabar (HgS) and sphalerite ((Zn,Fe,Mn)S) that developed during cooling of this solid solution (see also Powell and Pattison, 1997). Of the pure end-member phases, cinnabar has the lower melting point at 825°C (Kullerud, 1965), whereas pure ZnS melts at 1,680°C (e.g., Mavrogenes et al., 2001). Substitution of Zn in cinnabar increases the melting temperature of the solid solution (Osadchii, 1990). There is also potential for CuS, CdS, NiS, SnS, InS, and GaS solid solution in the sphalerite system at 600°C (Czamanske and Goff, 1973; Kojima and Sugaki, 1984; Osadchii, 1986, 1990, 1996; Ueno and Scott, 2002). Electron microprobe analyses of cinnabar-sphalerite exsolution lamellae show that the precursor solid solution contained only minor FeS and MnS (Table 1); and trace amounts of GaS, InS, and CuS are now detected in sphalerite.

Figure 9 shows that only about 1 to 2 percent FeS is present in sulfosalt melts containing Cu_2S, Sb_2S_3, As_2S_3, and PbS at 600°C (FeS_2 contributes similarly; Fig. 8J). Although there have been no studies that examined ZnS, HgS, or MnS in place of FeS, there is solid solution among these end members. Thus, these components may show behavior similar to that of FeS in the melting reactions. Because addition of HgS to (Zn,Fe,Mn)S significantly lowers the melting temperature of the solid solution (e.g., Fig. 10B), a HgS-rich solid solution would melt more when combined with sulfosalt melt than pure FeS or ZnS end members. This effect should also cause

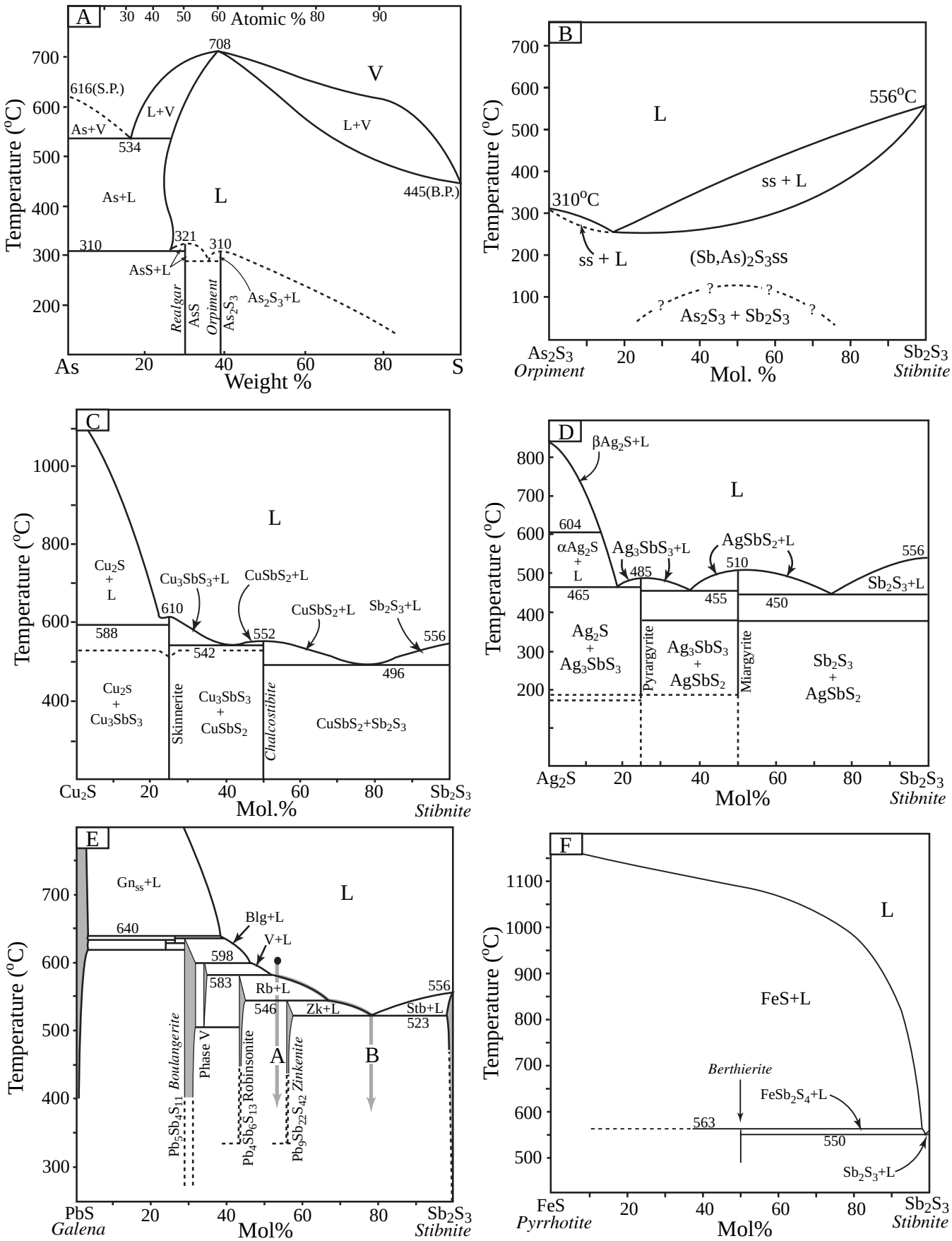
A
Atomic %
Temperature (°C)
Weight %
As
S
708
616(S.P.)
534
310
321
445(B.P.)
As+V
As+L
L+V
V
L
AsS+L
Realgar
AsS
Orpiment
As2S3
As2S3+L
B
556°C
310°C
ss + L
(Sb,As)2S3ss
As2S3 + Sb2S3
Mol. %
Orpiment
Stibnite
C
Cu2S + L
Cu3SbS3+L
CuSbS2+L
Sb2S3+L
610
588
552
542
496
556
Cu2S + Cu3SbS3
Skinnerite
Cu3SbS3 + CuSbS2
Chalcostibite
CuSbS2+Sb2S3
Mol.%
D
βAg2S+L
αAg2S + L
Ag3SbS3+L
AgSbS2+L
604
485
510
556
Sb2S3+L
465
455
450
Ag2S + Ag3SbS3
Pyrargyrite
Ag3SbS3 + AgSbS2
Miargyrite
Sb2S3 + AgSbS2
Mol%
E
Gnss+L
Blg+L
V+L
640
598
583
Rb+L
546
Zk+L
556
Stb+L
523
Boulangerite
Pb5Sb4S11
Phase V
Robinsonite
Pb4Sb6S13
Zinkenite
Pb9Sb22S42
PbS
Galena
F
FeS+L
Berthierite
FeSb2S4+L
563
550
Sb2S3+L
FeS
Pyrrhotite

preferential partitioning of Hg from the solid solution into the melt.

In the subsystem Fe-Mo-S (Fig. 10E), molybdenite and pyrite start to melt at 735°C (at 1 bar). The initial melting temperature clearly exceeds the peak metamorphic temperature reached at Hemlo, so a melting reaction between these two minerals is not expected. Although phase relations between molybdenite and the other sulfides are largely unknown, the paucity of molybdenite in association with Group II minerals suggests that it did not melt at the peak P-T conditions.

Melting relations in the system Au-Ag-Hg-As-Sb (S absent)

All of the components in the Au-Ag-Hg-As-Sb system are present at Hemlo as native elements and/or as intermetallic compounds (such as aurostibite, $AuSb_2$). All gold grains contain Ag and Hg in solid solution, and some of the gold grains lie in the $AuAgHg_{ss}$ + L field at 600°C (Fig. 11A–C). This means that even in the absence of other minerals, some of the gold grains from Hemlo would have partly melted during peak metamorphism. However, gold grains in the dilational zones typically coexist with many other phases, which further reduce their melting temperature.

Native arsenic rims a large proportion of gold grains in the dilational domains, although the rims are often very narrow (e.g., Figs. 6 and 7). Such grains would react to form gold and a Au-As melt. Or, if there was more than 32 percent As in an Au-As grain (e.g., Fig. 7A), the reaction products would be native arsenic and Au-As melt. Both reactions occur at 636°C in the pure system (Fig. 11D). Although the system Ag-As-Au-Hg has not been studied experimentally, it is probable that significant amounts of Hg and Ag in solid solution in gold would lower the eutectic temperature, possibly resulting in a wide compositional field for melt at 600°C.

Examination of the Au-Sb binary subsystem (Fig. 11E) reveals that native antimony is completely molten at 631°C, and when native antimony and aurostibite ($AuSb_2$) coexist, melting commences at 460°C. In this melting reaction, aurostibite is completely consumed and the melt becomes more Sb rich with increasing temperature. As an isolated phase, aurostibite melts at 460°C, but coexisting aurostibite and pure gold start to melt at only 360°C. Figure 7B and C shows examples from Hemlo of gold (with ~26% Hg and 5–9% Ag in solid solution) coexisting with aurostibite. The assemblage is present in late fractures within a D_2-boudinaged quartz vein (i.e., deformed at high temperature), consistent with a Au-rich melt persisting at Hemlo during retrograde cooling down to 360°C or less. At 600°C, a melt containing as much as 85 percent Au can exist in the Au-Sb binary system, indicating that Sb has a profound influence on melting of gold. Addition of Ag, Hg, and As to the Au-Sb system promotes even greater melting of gold. For example, As-Sb binary phase relations (Fig. 11F) show that addition of Sb lowers the melting point of As considerably (and vice versa). These phase relations suggest that at 600°C, only compositions along the Au-Ag join with little contamination from Hg, As, and Sb (as well as fairly pure native arsenic and antimony) would have remained solid. Therefore, most of the gold associations observed in dilational structures at Hemlo (Figs. 6 and 7) represent assemblages that would have been molten at peak metamorphic conditions.

Melting relations in the system Au-Ag-Hg-Sb-Pb-Ni-Te

The most important part of this system, in terms of understanding gold distribution at Hemlo, is the subsystem Au-Ag-Te, which has been studied extensively by experimentalists. The phase relations show that coexisting gold, calaverite ($AuTe_2$), and petzite ($AuAg_3Te_2$; all found at Hemlo) would start to melt below 335°C (Fig. 12), with the specific reactions depending on the starting composition. Figure 12A shows that in isolation, calaverite melts at 464°C; but in association

FIG. 8. Phase relations among sulfosalts in the system Sb-As-Tl-Pb-Ag-Cu-Fe-S at 1 bar. Phases identified at Hemlo are indicated in italics. A. Phase diagram of the system As-S (after Hansen and Aderko, 1958), showing that in isolation, realgar (AsS) and orpiment (As_2S_3) melt at 321° and 310°C (at 1 bar), respectively. Dashed lines on all diagrams indicate less certainty. B. Phase diagram of the system As_2S_3-Sb_2S_3 (orpiment-stibnite). This diagram was constructed from information in Sobott (1984). C. Phase diagram of the system Cu_2S-Sb_2S_3 at 1 bar (modified from Bryndzia and Davis, 1989). In this pure system, skinnerite (Cu_3SbS_3; T_m = 610°C) is analogous to the Cu-tetrahedrite end member ($Cu_{12}Sb_4S_{13}$) in more complex natural systems. D. Phase diagram of the system Ag_2S-Sb_2S_3 at 1 bar (after Bryndzia and Kleppa, 1988). In this pure system, pyrargyrite (Ag_3SbS_3; T_m = 485°C) is analogous to the Ag-tetrahedrite end member ($Ag_{12}Sb_4S_{13}$) in more complex natural systems. E. Phase diagram of the system PbS-Sb_2S_3 at 1 bar (after Salanci, 1979). Path A illustrates the compositional path followed during equilibrium crystallization of a given melt composition. Path B illustrates the compositional path followed by the same melt during ideal fractional crystallization. F. Phase diagram of the system FeS-Sb_2S_3. This diagram was constructed from information in Barton (1971), Figure 8J, and Urazov et al. (1983). G. Ternary section in the system As_2S_3-Sb_2S_3-Tl_2S (after Sobott, 1984), showing phase distribution at 315°C (at 1 bar). The lighter-shaded region represents the extent of the liquid field at 275°C. Note that (A) corresponds to the bottom join on this diagram. H. Ternary sections at 500° and 600°C in the system PbS-FeS-Sb_2S_3 (at 1 bar). The 500°C section is that given by Chang and Knowles (1977) and shows the subsolidus mineral phases in this system. The 600°C section was constructed from information in Chang and Knowles (1977) and Barton (1971). Although we do not know the extent of FeS melting, we suggest that it is likely that FeS contributes minimally to the melt composition, based on (F) and (J). I. Ternary section in the system As-Cu-S (modified from Maske and Skinner, 1971), showing the distribution of mineral phases and melt at 300°C, and the distribution of melt at 500°, 600°, and 665.5°C. A = unnamed compound, Cv = covellite, Dom = domeykite, En = enargite, fcc = face centered cubic, hcp = hexagonal closet packed, Lt = lautite, S = sinnerite. J. Liquidus surface map of the system Fe-Sb-S (after Barton, 1971). All of the fields in the detail to the right are + L_2. Note that there is only <1 percent $Fe_{1-x}S$ or FeS_2 in the melt at 600°C. The position of Figure 8F on this diagram corresponds to the join between FeS and Sb_2S_3. K. Ternary section in the system Cu_2S-PbS-Sb_2S_3 (after Pruseth et al., 1997), showing the distribution of minerals and melt at 500°C (at 1 bar). L. Ternary section in the system Ag_2S-PbS-Sb_2S_3 (after Hoda and Chang, 1975), showing the distribution of minerals and melt at 500°C (at 1 bar). The differences between the PbS-Sb_2S_3 axes of (H), (J), and (K) are due to differences in the published phase diagrams.

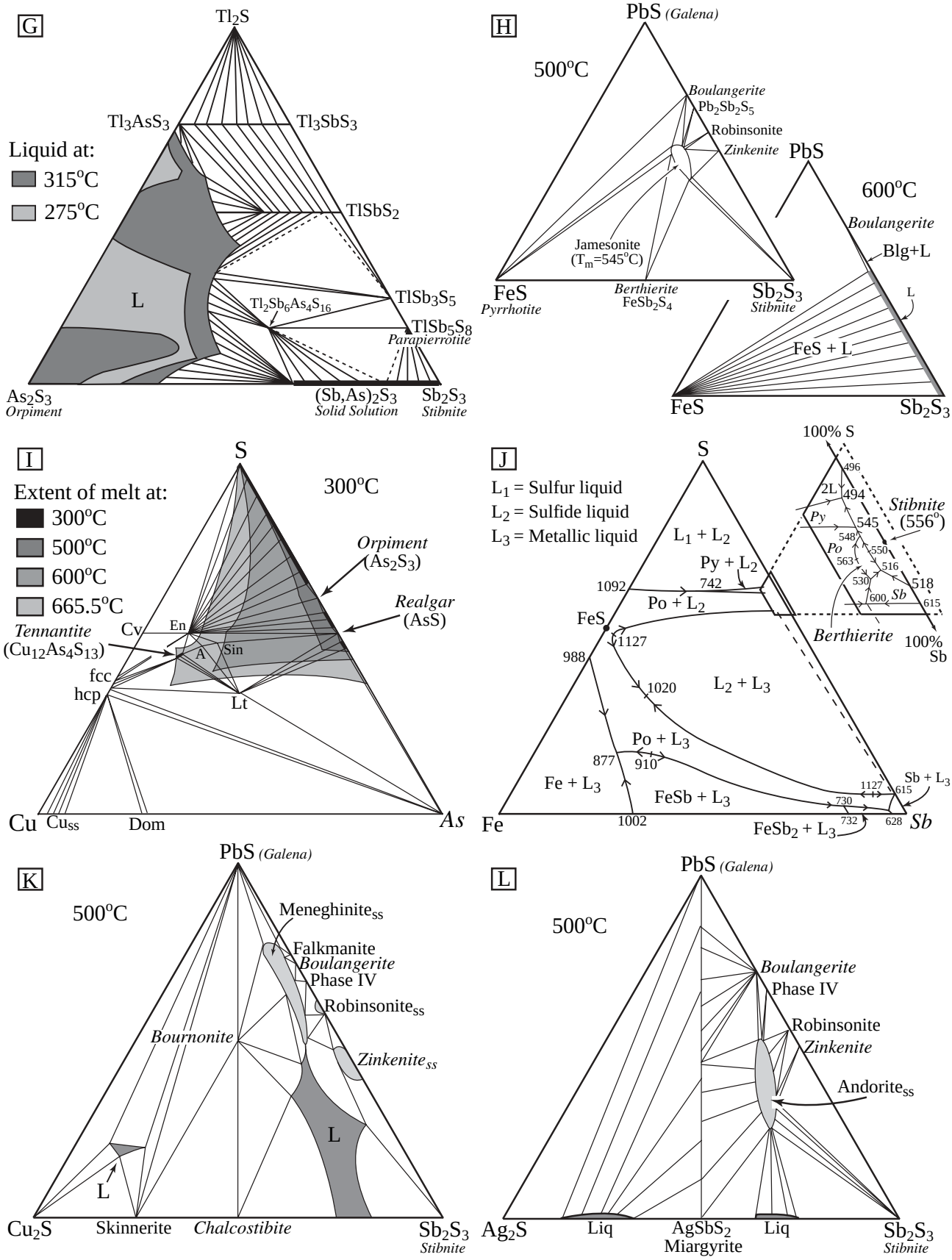
G
Tl2S
Tl3AsS3
Tl3SbS3
Liquid at:
315°C
275°C
TlSbS2
L
Tl2Sb6As4S16
TlSb3S5
TlSb5S8
Parapierrotite
As2S3
Orpiment
(Sb,As)2S3
Solid Solution
Sb2S3
Stibnite
H
PbS (Galena)
500°C
Boulangerite
Pb2Sb2S5
Robinsonite
Zinkenite
PbS
600°C
Boulangerite
Blg+L
L
Jamesonite
(Tm=545°C)
FeS
Pyrrhotite
Berthierite
FeSb2S4
Sb2S3
Stibnite
FeS + L
FeS
Sb2S3
I
S
300°C
Extent of melt at:
300°C
500°C
600°C
665.5°C
Orpiment
(As2S3)
Realgar
(AsS)
Tennantite
(Cu12As4S13)
Cv
En
A
Sin
fcc
hcp
Lt
Cu
Cuss
Dom
As
J
L1 = Sulfur liquid
L2 = Sulfide liquid
L3 = Metallic liquid
S
100% S
496
2L
494
Stibnite
(556°)
Py
545
548
Po
550
563
516
530
518
600
Sb
615
L1 + L2
Py + L2
742
1092
Po + L2
FeS
1127
Berthierite
100%
Sb
988
1020
L2 + L3
Po + L3
877
910
Fe + L3
FeSb + L3
1127
615
Sb + L3
730
Fe
1002
FeSb2 + L3
732
628
Sb
K
PbS (Galena)
500°C
Meneghinitess
Falkmanite
Boulangerite
Phase IV
Robinsonitess
Bournonite
Zinkenitess
L
L
Cu2S
Skinnerite
Chalcostibite
Sb2S3
Stibnite
L
PbS (Galena)
500°C
Boulangerite
Phase IV
Robinsonite
Zinkenite
Andoritess
Ag2S
Liq
AgSbS2
Miargyrite
Liq
Sb2S3
Stibnite

FIG. 8. *(Cont.)*

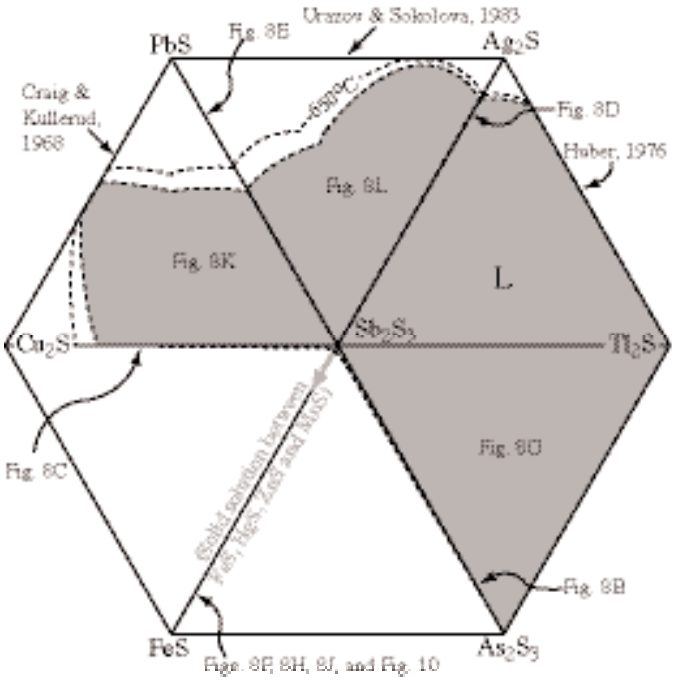

FIG. 9. Combined ternary sections at 600°C in the system Ag_2S-PbS-Cu_2S-FeS-As_2S_3-Tl_2S-Sb_2S_3, centered around Sb_2S_3, showing the approximate compositional extent of melt (gray-shaded area) at the peak metamorphic conditions for Hemlo. These are approximations based on the phase diagrams in Figure 8, as well as on information in Craig and Kullerud (1968), Huber (1983), and Urazov and Sokolova (1983). A contour showing the extent of melt at 650°C is also included. All end members in this system, except FeS, contribute significantly to a sulfide melt involving stibnite (Sb_2S_3) at 600°C. Components that form solid solutions with FeS (ZnS, HgS, MnS) may similarly contribute little to the melt, although components with a lower melting point than FeS (i.e., HgS, MnS) may widen the melt field to some unknown extent (gray arrow).

with gold, melting commences at 447°C. Melting points of most of the remaining telluride minerals found at Hemlo are unknown. However, the assemblage calaverite + altaite (PbTe) melts at <425°C (Legendre, 1990).

The effect of pressure

Nearly all of the experimental systems discussed above were determined at atmospheric pressure only, and the inadequacy of thermodynamic data for most of the sulfosalts makes it impossible to accurately calculate the high-pressure phase relations. Frost et al. (2002) suggested that increasing pressure in S-bearing systems leads to slightly higher melting temperatures, and two experimental studies bear this out. Mavrogenes et al. (2001) found that the eutectic temperature of the system FeS-PbS-ZnS increases by 6°C/kbar, and the temperature at which the reaction arsenopyrite + pyrite = AsS_{melt} + pyrrhotite proceeds, increases by 17°C/kbar (Clark, 1960); although data in Sharp et al. (1985) suggest that the increase may be closer to 14°C/kbar. However, Roland (1968) found that the temperature of the reaction jordanite = galena + Pb-As-S_{melt} did not vary with pressure within the uncertainty of measurement.

For Sb-bearing systems, Frost et al. (2002) suggested that increasing P may lead to lower melting temperatures, because the melting temperature of pure Sb decreases with increasing pressure (–0.2°C/kbar; Liu and Bassett, 1986). For the S-absent system Ag-As-Au-Hg-Sb, this may lead to slightly reduced melting temperatures at higher pressures. Similarly, the melting temperature of Sb_2S_3 and the other Sb-sulfosalts may be less affected by pressure than are most other sulfides and sulfosalts, although this has not been experimentally determined. The melting temperature of pure Te is less affected by pressure (1.5°C/kbar) than that of pure S (13.8°C/kbar; Liu and Bassett, 1986), suggesting that melting temperatures of tellurides may be less sensitive to pressure than that of sulfides.

Implications for mobilization

Consideration of published, experimental evidence suggests that the assemblage of ore minerals in the dilational domains (the group II minerals) is consistent with having crystallized from a complex sulfosalt-dominated melt. In contrast, the ore mineral assemblages in the higher strain, compressional domains (the group I minerals) are unlikely to have melted. This implies that sulfosalt melts were mobilized from higher strain regions into dilational sites during syn- to late-peak metamorphism (D_2 and D_3 structures), whereas refractory sulfides were not extensively mobilized. Evidence for localized hydrothermal alteration associated with some dilational sulfosalt-bearing structures (Muir, 2002) is not inconsistent with a melting model, because any hydrothermal fluid present would be expected to migrate to the same structural sites, and perhaps even deposit minor amounts of metal. Based on the amount of sulfosalt minerals in the deposit, we estimate that the sulfosalt melt volume at the peak of metamorphism may have been <2 percent of the rock volume.

Discussion

Premetamorphic ore mineral assemblage

It is likely that metamorphism and melting significantly modified the premetamorphic ore mineral assemblage. The rare examples of unmetamorphosed ore deposits with bulk geochemistry similar to that of the Hemlo ores (e.g., Lake George: Seal et al., 1988; Nizke Tatry: Chavan et al., 1995) contain pyrite, molybdenite, stibnite, pyrrhotite, arsenopyrite, native antimony, gold, sphalerite, galena, tetrahedrite, bornite, and chalcopyrite. It is likely that many of these minerals, in addition to cinnabar, were present prior to metamorphism at Hemlo. The group I minerals at Hemlo were probably part of this original mineral assemblage. Although it is difficult to rule out that realgar and orpiment were also part of the original mineral assemblage, the presence of arsenopyrite in the unmetamorphosed deposits suggests that it was the important As mineral in the premetamorphic assemblage (orpiment, realgar, and arsenopyrite cannot coexist in equilibrium; Fig. 13). The preservation of arsenopyrite in the wall rocks at Hemlo supports this interpretation (the fate of arsenopyrite during metamorphism is discussed below). The rarer elements may have resided as substitutions in the more common sulfides (e.g., Ag and Tl in galena), or as included rare minerals.

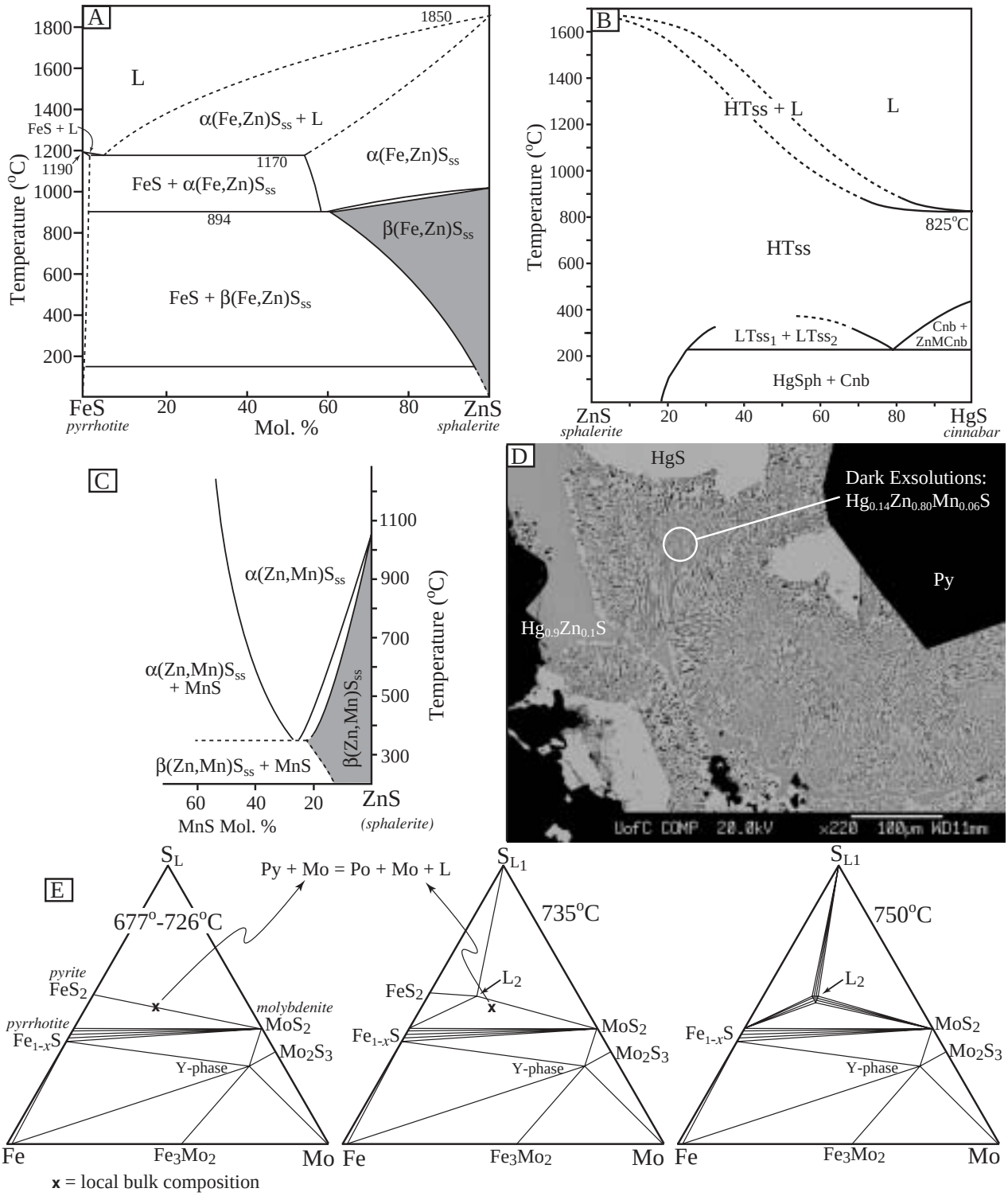

FIG. 10. Phase relations among the refractory sulfides in the system MoS_2-FeS_2-FeS-ZnS-HgS-MnS at 1 bar. Phases identified at Hemlo are indicated in italics. A. Phase relations in the system FeS-ZnS (after Kullerud, 1953), showing the extent of solid solution (at 150 bar). B. Phase relations in the system ZnS-HgS (at 1 bar). This diagram is partly derived from Powell and Pattison (1997), and partly from Osadchii (1990). Note that above ~425°C there is complete solid solution between ZnS and HgS, and that melting commences at the pure HgS end member at 825°C. Cnb = cinnabar, HgSph = mercurian sphalerite, HTss = high-temperature solid solution, LTss = low-temperature solid solution, ZnMCnb = zincian metacinnabar. C. Phase relations in the system ZnS-MnS (after Tauson et al., 1977), showing the extent of solid solution (at 1 kbar). D. Backscattered electron image of phases exsolved from HgS-ZnS-MnS solid solution at Hemlo. E. Phase relations in the system Fe-Mo-S (after Grover et al., 1975). Three ternary sections at 677° to 726°, 735°, and 750°C (all at 1 bar pressure) show the commencement of melting between pyrite (FeS_2) and molybdenite (MoS_2) by the reaction Py + Mo = Po + Mo + L.

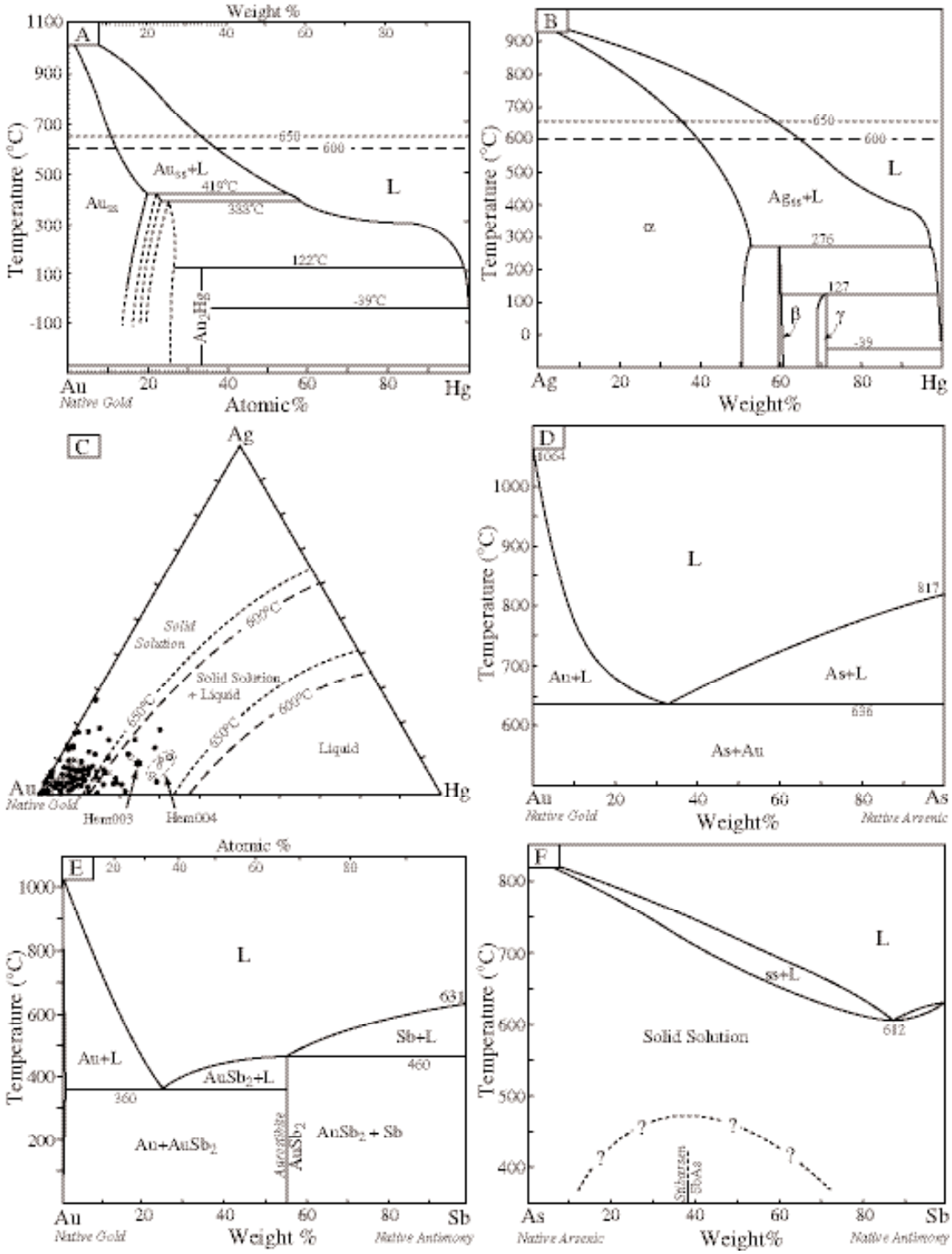

FIG. 11. Phase relations in the sulfur-absent system Au-Ag-Hg-As-Sb at 1 bar. Phases identified at Hemlo are indicated in italics. A. Au-Hg phase diagram (after Okamoto and Massalski, 1986a). This diagram corresponds to the bottom join in (C). B. Ag-Hg phase diagram (after Hansen and Aderko, 1958). This diagram corresponds to the right join in (C). C. Au-Ag-Hg ternary diagram constructed from (A) and (B), showing the approximate positions of the solid solution, solid solution + liquid, and liquid fields at 600° and 650°C. Also plotted are compositions of gold grains from this study (open circles), from Harris (1989; closed circles), and from Williams-Jones et al. (unpub. report for Canadian Mining Industry Research Organization, 1998; crosses). The star represents the composition of a gold grain from sample AGT-Hem003, which is shown in Fig. 6D. The range of gold composition in sample AGT-Hem004 (shown in Fig. 7B and C) is also indicated. D. Au-As phase diagram (after Okamoto and Massalski, 1986b). E. Au-Sb phase diagram (after Okamoto and Massalski, 1986c). F. As-Sb phase diagram (after Hansen and Aderko, 1958).

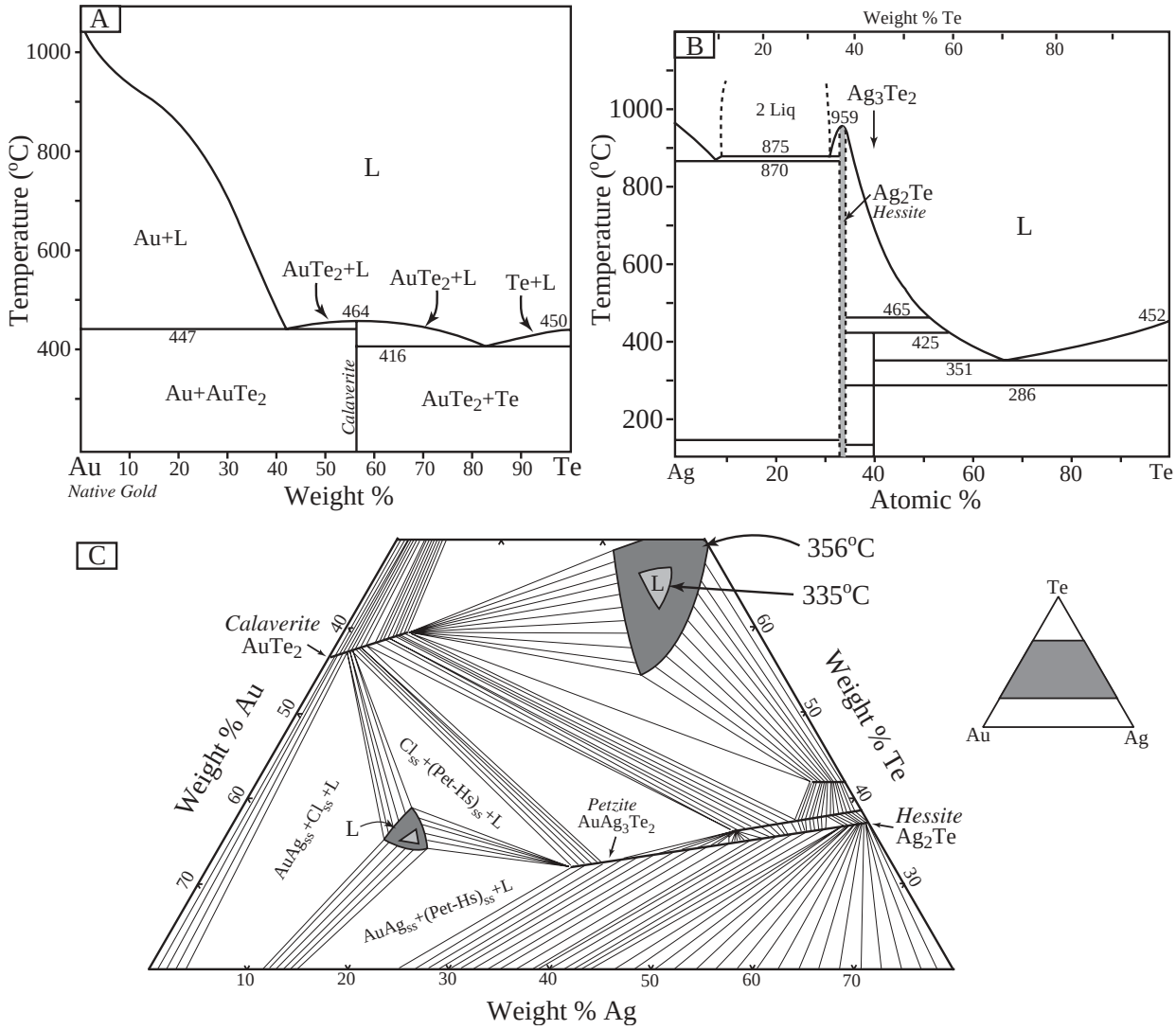

FIG. 12. Phase relations in the system Ag-Au-Te at 1 bar. Phases identified at Hemlo are indicated in italics. A. Au-Te phase diagram (after Okamoto and Massalski, 1986d). B. Ag-Te phase diagram (after Hansen and Aderko, 1958). C. Ternary section of the system Ag-Au-Te, showing the distribution of mineral phases and melt at 356°C, with an additional melt contour at 335°C (after Cabri, 1965).

Formation and migration of the sulfosalt melt

Of the original ore mineral suite, we believe that the most important contributors to the melt (in terms of melt volume) were stibnite and arsenopyrite, because Sb- and As minerals are dominant in all dilational domains. The relative abundance of arsenopyrite in the hanging-wall rocks and compared to the ore zones suggests that it may have been consumed within the orebody during prograde metamorphism. Melting of stibnite, even as an isolated phase, would have occurred when the temperature exceeded ~556°C (depending slightly on the pressure). However, arsenopyrite melting is dependent on f_{S_2} (e.g., Clark, 1960), which is buffered during prograde metamorphism by a combination of desulfidation reactions and reactions involving silicate minerals (Tracy and Robinson, 1988; Seal et al., 1990; Craig and Vokes, 1993). The persistence of pyrite throughout the deposit indicates that f_{S_2} must have been high at peak metamorphic conditions, beyond the stability field of arsenopyrite, and that arsenopyrite melting is a reasonable possibility (Fig. 13). This melting would have proceeded by two possible reactions:

$$(1) \quad FeAsS + FeS_2 = As\text{-}S_{(liquid)} + 2FeS$$

$$(2) \quad FeAsS + S_2 = As\text{-}S_{(liquid)} + FeS_2$$

Reaction 1 takes place on the pyrite-pyrrhotite buffer and results in the formation of pyrrhotite as a solid by-product. Therefore, the occurrence of this reaction would be recorded by the presence of pyrrhotite in the final assemblage, but in fact pyrrhotite is only locally observed. Reaction 2 implies the consumption of some other S-bearing mineral, liberating S. Of the two other widely distributed S-bearing minerals at Hemlo (molybdenite and barite; Harris, 1989), only barite is likely to have been consumed during metamorphism. Most of

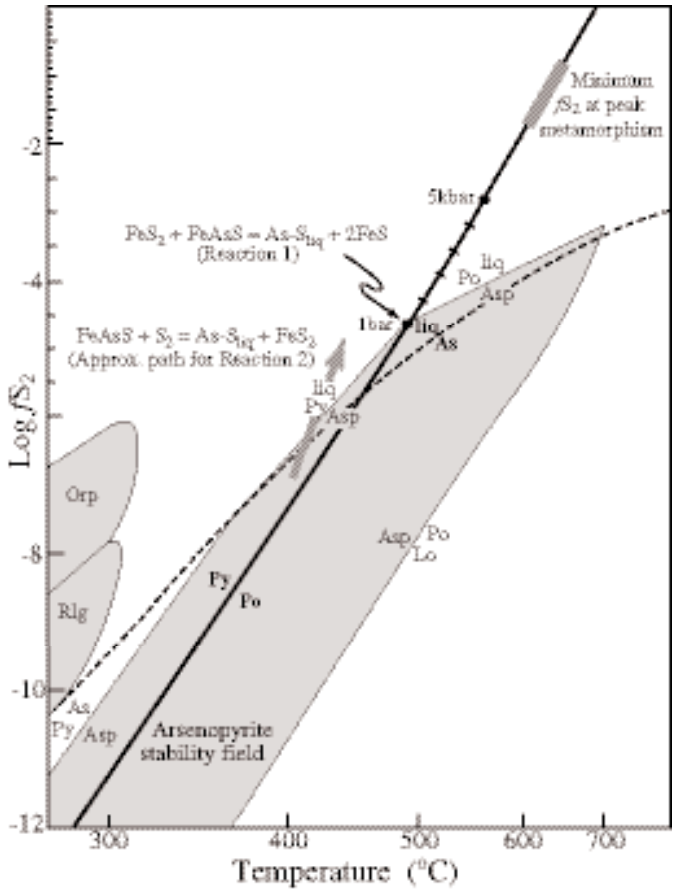

FIG. 13. f_{S_2}-temperature grid showing the stability fields of arsenopyrite, realgar, and orpiment (shaded areas), and the position of two arsenopyrite melting reactions. Original experimental work conducted by Barton (1969); 5 kbars pressure constraint determined by Sharp et al. (1985). Note the minimum f_{S_2} conditions estimated for peak metamorphism at Hemlo, based on the widespread persistence of pyrite. The dashed curve divides the diagram into two fields; above this line, As is only stable as a liquid (with sulfur) at moderate to high temperature, whereas below it is stable as a solid.

the widely distributed barian K-feldspar grains at Hemlo show consistent concentric zoning with wide low-Ba cores and high-Ba margins (Fig. 4C). These typically display a granoblastic texture with ~120° triple junctions, suggesting additional metamorphic growth and equilibration in a Ba-enriched environment. This implies that barite was consumed during metamorphism at Hemlo, thus releasing S for arsenopyrite melting by reaction 2.

An As-Sb-S melt would have been highly mobile during deformation due to its low viscosity. This would have enabled it to physically and chemically interact with the other ore minerals (by wetting grain boundaries), promoting further partial melting. Some elements, such as Hg, Ag, and Tl, may have partitioned into the melt from refractory solid-solution phases (e.g., Frost et al, 2002). The fact that many of the group II sulfosalts contain significant Hg, but little Fe or Zn, suggests that Hg was preferentially partitioned into the melt.

As each individual melt globule migrated during deformation, it would have interacted with only the ore minerals in its immediate environment, leading to a wide range of local bulk compositions. This would have led to significant compositional heterogeneity between melt accumulations, although, due to the abundance of pyrite at Hemlo, it is likely that all melts would have been saturated in FeS_2 (at ~1–2%; Fig. 8J).

Figure 11 shows the importance of Sb and As in lowering the melting point of gold. Thus, it is probable that gold was incorporated and mobilized within the early-formed Sb- and As-rich sulfosalt melts. This interpretation is supported by the observation of both Sb- and As-bearing sulfosalts in contact with gold in many dilational domains (Figs. 5, 6, and 7).

Because the sulfosalt melts only made up <2 percent of the rock, they could not coalesce into one large accumulation, particularly since they came from an originally disseminated and widely dispersed distribution within the deposit. However, the melts did coalesce locally within dilational sites (e.g., Fig. 5 shows a 3-cm-wide accumulation of stibnite-dominated sulfosalt material). Although there was some tendency toward homogenization of the melts, we have found that each accumulation has a unique composition.

Evolution of the complex ore mineral assemblage during cooling

Because the melt volume was low, there was limited interconnectivity between individual melt accumulations. Each accumulation would therefore have been internally buffered and controlled by the immediate bulk-rock composition. It is possible to predict cooling paths for simple assemblages. During equilibrium crystallization, each aliquot of melt would crystallize a relatively simple assemblage (e.g., path A; Fig. 8E). However, during fractional crystallization, melts would evolve toward eutectic compositions and continually crystallize additional phases (e.g., path B; Fig. 8E). In this way, fractional crystallization, induced by late episodes of deformation (probably associated with D_3, D_4, and D_5), may have led to the very low melting-temperature mineral associations. With more components, the array of possible crystallization paths is multiplied, consistent with the large range of assemblages observed. This would account for the late realgar-coated fractures and the array of rare sulfosalt phases in fractures propagating from coarse stibnite and/or realgar clots (Figs. 5 and 6).

Because the interpreted bulk composition of melt accumulations at Hemlo was dominated by antimony, stibnite is likely to have crystallized early. However, because all sulfosalt melts are likely to have been saturated in FeS_2, very small amounts of pyrite, berthierite, or pyrrhotite are expected to have been the first phases to crystallize in most instances. As crystallization of stibnite progressed, the remaining melt would have become enriched in the other elements. Arsenic also was likely abundant in the melt, but Figure 8B indicates that arsenic must be extremely enriched in the melt before realgar or orpiment could be the first to crystallize. Therefore, most sulfosalt melt accumulations are likely to have evolved toward Sb-poor and As-rich compositions. This explains why realgar is common in the last stages of mobilization and crystallization at Hemlo. Of the other elements found in the sulfosalt assemblage, Zn-bearing minerals are likely to have crystallized early, and Hg-, Cu-, and Pb-bearing sulfosalts next, with Tl being concentrated in the last vestiges of melt. As a very approximate melt evolution sequence,

we suggest the following order of depletion from the melt (or order of crystallization) for most sulfosalt melt accumulations at Hemlo: Zn → Fe → Hg → Sb → Pb → Ag → Cu → As → Tl. Although Hg and Sb may be depleted early in the sequence, enough must have remained in the melt to account for the high Hg and Sb content of the Tl-bearing sulfosalts at Hemlo (Fig. 8G). Gold is likely to have continually crystallized during cooling, down to temperatures slightly lower than 335°C (Figs. 11 and 12).

Implications for mining and exploration at Hemlo

An auriferous sulfosalt melt, like any ore-bearing fluid, would be expected to have migrated along the Hemlo shear zone and not away from it (north or south). Fluids within shear zones are preferentially focused into dilational regions, such as jogs, and they are mainly expelled at the terminus of the shear zone or at splays, rather than escaping laterally into the wall rocks (e.g., Cox et al., 2001).

We have shown that pockets of sulfosalt melt were likely trapped at meso- and microscale dilational sites up to 1.5 m in size. Larger-scale features (meter to hundreds of meters) into which greater volumes of melt could have migrated might also have been present. Prospective structures within or close to the mineralized zone would therefore include megaboudins within larger competent units (such as premetamorphic dikes), fault-related jogs in the contact between the metasediments and the Moose Lake porphyry, and perhaps the hypothetical saddle between these same units in the nose of the isoclinal fold proposed by Lin (2001). This last structure, if it existed, may have been destroyed by progressive shearing, as is commonly observed in isoclinal fold systems.

The low viscosity of sulfide melts means that they could potentially migrate long distances (tens of kilometers). However, the predicted volume of melt at Hemlo was small (<2% of the rock volume), and there are a large number of small dilational domains within the rock volume, so it is possible that most of the melt only migrated a short distance to the nearest dilational site. In this way, we suggest that the process of sulfide melting at Hemlo may have produced a nugget effect, where small pockets of very high grade gold are dispersed within large volumes of average-grade ore material.

Acknowledgments

The assistance of Hugh Lockwood and Dave Truscott at the Golden Giant mine, and Gord Skrecky at the Williams mine, in viewing the Hemlo orebody and obtaining samples is greatly appreciated. Mark Smyk at the Ontario Geological Survey is also thanked for providing samples from Hemlo. A.E. Williams-Jones and Yuanming Pan are thanked for providing excellent reviews. Funding for this project was provided by an Alberta Ingenuity Fellowship to A.G.T. and NSERC Discovery Grant 037233 to D.R.M.P. We recognize that Martin Heiligmann of McGill University also independently arrived at the conclusion that some components of the ore assemblage at Hemlo melted, a fact that we only became aware of when this manuscript was reviewed by his Ph.D. supervisor, A.E. Williams-Jones.

August 12, 2003; June 4, 2004

REFERENCES

Barton, P.B. Jr., 1969, Thermodynamic study of the system Fe-As-S: Geochimica et Cosmochimica Acta, v. 33, p. 841–857.

——1971, The Fe-Sb-S system: Economic Geology, v. 66, p. 121–132.

Bodycomb, V., Williams-Jones, A.E., and Clark, J.R., 2000, The Archean Hemlo gold deposit, Ontario, Canada: Alteration, mineralization, and lithogeochemistry [abs.]: Geological Association of Canada, Extended Abstracts 25 (on CD).

Bryndzia, L.T., and Davis, A.M., 1989, Liquidus phase relations on the quasi-binary join Cu2S-Sb2S3: Implications for the formation of tetrahedrite and skinnerite: American Mineralogist, v. 74, p. 236–242.

Bryndzia, L.T., and Kleppa, O.J., 1988, High-temperature reaction calorimetry of solid and liquid phases in the quasi-binary system Ag_2S-Sb_2S_3: Geochimica et Cosmochimica Acta, v. 52, p. 167–176.

Burk, R., Hodgson, C.J., and Quatermain, R.A., 1986, The Geological setting of the Teck-Corona Au-Mo-Ba deposit, Hemlo, Ontario, Canada: Konsult International, Gold '86, Toronto, Ontario, 1986, Proceedings, p. 311–326.

Cabri, L.J., 1965, Phase relations in the Au-Ag-Te system and their mineralogical significance: Economic Geology, v. 60, p. 1569–1606.

Cameron, E.M., and Hattori, K., 1985, The Hemlo gold deposit, Ontario: A geochemical and isotopic study: Geochimica et Cosmochimica Acta, v. 49, p. 2041–2050.

Chang, L.L.Y., and Knowles, C.R., 1977, Phase relations in the systems PbS-$Fe_{1-x}S$-Sb_2S_3 and PbS-$Fe_{1-x}S$-Bi_2S_3: Canadian Mineralogist, v. 15, p. 374–379.

Chavan, M., Hurai, V., Sachan, H.K., and Kantor, J., 1995, Origin of the fluids associated with granodiorite-hosted, Sb-As-Au-W mineralization at Dubrava (Nizke Tatry Mts., Western Carpathians): Mineralium Deposita, v. 30, p. 48–54.

Clark, L.A., 1960, The Fe-As-S system: Phase relations and applications, part II: Economic Geology, v. 55, p. 1631–1652.

Corfu, F., and Muir, T.L., 1989, The Hemlo-Heron Bay greenstone belt and Hemlo Au-Mo deposit, Superior province, Ontario, Canada: 2. Timing of metamorphism, alteration, and Au mineralization from titanite, rutile, and monazite U-Pb geochronology: Chemical Geology, v. 79, p. 201–223.

Cox, S.F., Knackstedt, M.A., and Braun, J., 2001, Principles of structural control on permeability and fluid flow in hydrothermal systems: Reviews in Economic Geology, v. 14, p. 1–24.

Craig, J.R., and Kullerud, G., 1968, Phase relations and mineral assemblages in the copper-lead-sulfur system: American Mineralogist, v. 53, p. 145–161.

Craig, J.R., and Vokes, F.M., 1993, The metamorphism of pyrite and pyritic ores: An overview: Mineralogical Magazine, v. 57, p. 3–18.

Czamanske, G.K., and Goff, F.E., 1973, The character of Ni^{2+} as demonstrated by solid solutions in the Ni-Fe-Zn-S system: Economic Geology, v. 68, p. 258–268

Davis, D.W., and Lin, S., 2003, Unravelling the geologic history of the Hemlo Archean gold deposit, Superior province, Canada: A U-Pb geochronological study: Economic Geology, v. 98, p. 51–67.

Dobson, D.P., Crichton, W.A., Vocaldo, L., Jones, A.P., Wang, Y., Uchida, T., Rivers, M., Sutton, S., and Brodholt, J.P., 2000, In situ measurement of viscosity of liquids in the Fe-FeS system at high pressures and temperatures: American Mineralogist, v. 85, p. 1838–1842.

Fleet, M.E., and Pan, Y., 1995, Magmatism, metamorphism, and deformation at Hemlo, Ontario, and the timing of Au-Mo mineralization in the Golden Giant mine—a discussion: Economic Geology, v. 90, p. 1338–1341.

Frost, B.R., Mavrogenes, J.A., and Tomkins, A.G., 2002, Partial melting of sulfide ore deposits during medium- and high-grade metamorphism: The Canadian Mineralogist, v. 40, p. 1–18.

Goldie, R., 1985, The sinters of the Ohaki and Champagne pools, New Zealand: Possible modern analogues of the Hemlo gold deposit, Northern Ontario: Geoscience Canada, v. 12, p. 60–64.

Grover, B., Kullerud, G., and Moh, G.H., 1975, Phase equilibrium conditions in the ternary Fe-Mo-S system in relation to natural minerals and ore deposits: Neues Jahrbuch Mineralogie. Abhandlungen, v. 124, p. 246–272.

Gustafson, L.B., 1995, Magmatism, metamorphism, and deformation at Hemlo, Ontario, and the timing of Au-Mo mineralization in the Golden Giant mine—a discussion: Economic Geology, v. 90, p. 1341–1342.

Hanson, M., and Aderko, K., 1958, Constitution of binary alloys: New York, McGraw-Hill, 1305 p.

Harris, D.C., 1989, The mineralogy and geochemistry of the Hemlo gold deposit, Ontario: Geological Survey of Canada, Economic Geology Report 38, 88 p.

Hattori, K., 1987, Magnetic felsic intrusions associated with Canadian Archean gold deposits: Geology, v. 15, p. 1107–1111.
Hoda, S.N., and Chang, L.L.Y., 1975, Phase relations in the systems PbS-Ag_2S-Sb_2S_3 and PbS-Ag_2S-Bi_2S_3: American Mineralogist, v. 60, p. 621–633.
Hofmann, B.A., 1994, Formation of a sulfide melt during alpine metamorphism of the Legenbach polymetallic sulfide mineralization, Bintal, Switzerland: Mineralium Deposita, v. 29, p. 439–442.
Huber, H., 1983, The system Ag_2S-Tl_2S, *in* Brandes, E.A., ed., Metals reference book, 6th edition: London and Boston, Butterworths-Heinman, p. 519.
Hugon, H., 1986, The Hemlo gold deposit, Ontario, Canada: A central portion of a large-scale, wide zone of heterogeneous ductile shear: Konsult International, Gold '86, Toronto, Ontario, 1986, Proceedings, p. 379–387.
Johnston, P.J., 1996, The geological setting of the Hemlo gold deposit, Ontario, Canada: Unpublished Ph.D. thesis, Ontario, Canada, Queens University, 297 p.
Johnston, P.J., and Smyk, M.C., 1992, The anatomy of the Hemlo Au-Mo deposit, Ontario [abs.]: Geological Association of Canada–Mineralogical Association of Canada, Abstract Volume 17, p. A53.
Kojima, S., and Sugaki, A., 1984, Phase relations in the central portion of the Cu-Fe-Zn-S system between 800° and 500°C: Mineralogical Journal, v. 12, p. 15–28.
Kuhns, R.J., 1986, Alteration styles and trace element dispersion associated with the Golden Giant deposit, Hemlo, Ontario, Canada: Konsult International, Gold '86, Toronto, Ontario, 1986, Proceedings, p. 340–354.
——1988, The Golden Giant deposit, Hemlo, Ontario: Geologic and geochemical relationships between mineralization, metamorphism, alteration, magmatism, and tectonism: Unpublished Ph.D. thesis, Minnesota, University of Minnesota, 458 p.
Kuhns, R.J., Sawkins, F.J., and Ito, E., 1994, Magmatism, metamorphism, and deformation at Hemlo, Ontario, and the timing of Au-Mo mineralization in the Golden Giant mine: Economic Geology, v. 89, p. 720–756.
Kullerud, G., 1953, The FeS-ZnS system: A geological thermometer: Norsk Geologisk Tidsskrift, v. 32, p. 61–147.
——1965, The Hg-S System: Carnegie Institute of Washington Yearbook, v. 64, p. 194.
Legendre, B., 1990, The system Au-Pb-Te, *in* Prince, E., Raynor, G.V., and Evans, D.S., eds., Phase diagrams of ternary gold alloys: London, The Institute of Metals, 550 p.
Lin, S., 2001, Stratigraphic and structural setting of the Hemlo gold deposit, Ontario, Canada: Economic Geology, v. 96, p. 477–507.
Liu, L-G., and Bassett, W.A., 1986, Elements, oxides, and silicates: High-pressure phases with implications for the Earth's interior: New York, Oxford University Press, 250 p.
Marshall, B., Vokes, F.M., and Larocque, A.C.L., 2000, Regional metamorphic remobilization: Upgrading and formation of ore deposits: Reviews in Economic Geology, v. 16, p. 19–38.
Maske, S., and Skinner, B.J., 1971, Studies of the sulfosalts of copper I: Phases and phase relations in the system Cu-As-S: Economic Geology, v. 66, p. 901–918.
Masliwec, A., McMaster, D., and York, D., 1986, The dating of Ontario's gold deposits: Geological Survey Miscellaneous Paper, v. 130, p. 107–114.
Mavrogenes, J.A., MacIntosh, I.W., and Ellis, D.J., 2001, Partial melting of the Broken Hill Galena-Sphalerite ore—experimental studies in the system PbS-FeS-ZnS-(Ag_2S): Economic Geology, v. 96, p. 205–210.
Michibayashi, K., 1995, Two phase syntectonic gold mineralization and barite remobilization within the main orebody of the Golden Giant mine, Hemlo, Ontario, Canada: Ore Geology Reviews, v. 10, 31–50.
Muir, T.L., 1997, Precambrian geology, Hemlo gold deposit area: Ontario Geological Survey Report 289, 219 p.
——2002, The Hemlo gold deposit, Ontario, Canada: Principal deposit characteristics and constraints on mineralization: Ore Geology Reviews, v. 21, p. 1–66.
——2003, Structural evolution of the Hemlo greenstone belt in the vicinity of the world-class Hemlo gold deposit: Canadian Journal of Earth Sciences, v. 40, p. 395–430.
Okamoto, H., and Massalski, T.B., 1986a, Au-Hg (gold-mercury): American Society for Metals, Ohio, v. 1, p. 265 and 267.
——1986b, As-Au (arsenic-gold): American Society for Metals, Ohio, v. 1, p. 191–192.
——1986c, Au-Sb (gold-antimony): American Society for Metals, Ohio, v. 1, p. 305 and 308–309.
——1986d, Au-Te (gold-tellurium): American Society for Metals, Ohio, v. 1, p. 322–323.
Osadchii, E.G., 1986, Solid solutions and phase relations in the system Cu_2SnS_3-ZnS-CdS at 850° and 700°C: Neues Jahrbuch Mineralogie. Abhandlungen, v. 155, p. 23–38.
——1990, The kesterite-velikite ($Cu_2Zn_{1-x}Hg_xSnS_4$) and sphalerite-metacinnabarite ($Zn_{1-x}Hg_xS$) solid solutions in the system Cu_2SnS_3-Zn-HgS at temperatures of 850°, 700°, and 550°C: Neues Jahrbuch Mineralogie. Monatshefte, v. H1, p.13–34.
——1996, Solid solutions kesterite-Mn-stannite and sphalerite-alabandite in the pseudoternary system Cu_2SnS_3-ZnS-MnS at 820° and 700°C: Neues Jahrbuch fuer Mineralogie. Monatshefte, v. 5, p. 201–211.
Pan, Y., and Fleet, M.E., 1992, Calc-silicate alteration in the Hemlo gold deposit, Ontario: Mineral assemblages, P-T-X constraints and significance: Economic Geology, v. 87, p. 1104–1120.
——1995, The late Archean Hemlo gold deposit, Ontario, Canada: A review and synthesis: Ore Geology Reviews, v. 9, p. 455–488.
Powell, W.G., and Pattison, D.R.M., 1997, An exsolution origin for low-temperature sulfides at the Hemlo gold deposit, Ontario, Canada: Economic Geology, v. 92, p 569–577.
Powell, W.G., Pattison, D.R.M., and Johnston, P., 1999, Metamorphic history of the Hemlo gold deposit from Al_2SiO_5 mineral assemblages, with implications for the timing of mineralization: Canadian Journal of Earth Sciences, v. 36, p. 33–46.
Pruseth, K.L., Mishra, B., and Bernhardt, H.J., 1997, Phase relations in the Cu_2S-PbS-Sb_2S_3 system: An experimental appraisal and application to natural polymetallic sulfide ores: Economic Geology, v. 92, p. 720–732.
Roland, G.W., 1968, The system Pb-As-S: Mineralium Deposita, v. 3, p. 249–260.
Salanci, B., 1979, Contribution to the system PbS-Sb_2S_3 in relation to lead-antimony-sulfosalts (in German): Neues Jahrbuch fuer Mineralogie. Abhandlungen, v. 135, p. 315–326.
Schnieders, B.R., Scott, J.F., Smyk, M.C., and O'Brian, M.S., 2000, Report of activities, 1999: Ontario Geological Survey, Open File Report 6005, 51 p.
Seal, R.R. II, Clark, A.H., and Morrissy, C.J., 1988, Lake George, southwestern New Brunswick: A Silurian, multi-stage, polymetallic (Sb-W-Mo-Au-base metal) hydrothermal centre: Canadian Institute of Mining and Metallurgy Special Volume 39, p. 252–264.
Seal, R.R. II, Essene, E.J., and Kelly, W.C., 1990, Tetrahedrite and tennantite: Evaluation of thermodynamic data and phase equilibria: Canadian Mineralogist, v. 28, p. 725–738.
Sharp, Z.D., Essene, E.J., and Kelly, W.C., 1985, A re-examination of the arsenopyrite geothermometer: Pressure considerations and applications to natural assemblages: Canadian Mineralogist, v. 23, p. 517–534.
Sobott, R.J.G., 1984, Sulfosalts and Tl_2S-As_2S_3-Sb_2S_3-S phase relations: Neues Jahrbuch fuer Mineralogie. Abhandlungen, v. 150, p. 54–59.
Tauson, V.L., Chernyshev, L.V., and Markeyev, A.B., 1977, Phase relations and structural characteristics of mixed crystals in the system ZnS-MnS: Geochemistry International, v. 14, p. 33–45.
Thode, H.G., Ding, T., and Crocket, J.H., 1991, Sulfur-isotope and elemental geochemistry studies of the Hemlo gold mineralization, Ontario: Sources of sulfur and implications for the mineralization process: Canadian Journal of Earth Sciences, v. 28, p. 13–25.
Tomkins, A.G., and Mavrogenes, J.A., 2002, Mobilization of gold as a polymetallic melt during pelite anatexis at the Challenger gold deposit, South Australia: A metamorphosed Archean deposit: Economic Geology, v. 97, p. 1249–1271.
Tracy, R.J., and Robinson, P., 1988, Silicate-sulfide-oxide-fluid reactions in granulite-grade pelitic rocks, central Massachusetts: American Journal of Science, v. 288A, p. 45–74.
Ueno, T., and Scott, S.D., 2002, Phase equilibria in the system Zn-Fe-Ga-S at 900° and 800°C: Canadian Mineralogist, v. 40, p. 563–570.
Urazov, G.G., and Sokolova, M.A., 1983, The system Ag_2S-PbS, *in* Brandes, E.A., ed., Metals reference book, 6th edition: London and Boston, Butterworths-Heinman, p. 525.
Urazov, G.G., Bol'shakov, K.A., Federov, P.I., and Vasilevskeya, I.I., 1983, The system FeS-Sb_2S_3, *in* Brandes, E.A., ed., Metals reference book, 6th edition: London and Boston, Butterworths-Heinman, p. 526.
Valliant, R.I., and Bradbrook, C.J., 1986, Relationship between stratigraphy, faults, and gold deposits, Page-Williams mine, Hemlo, Ontario, Canada: Konsult International, Gold '86, Toronto, Ontario, 1986, Proceedings, p. 355–361.

Walford, P.C., Stephens, J., Skrecky, G., and Barnett, R., 1986, The geology of the "A" zone, Page-Williams mine, Hemlo, Ontario, Canada: Konsult International, Gold '86, Toronto, Ontario, 1986, Proceedings, p. 362–368.

Williams, H.R., Heather, K.B., Muir, T.L., Sage, R.P., and Scott, G.S., 1991, Wawa subprovince: Ontario Geological Survey Special Volume 4, p. 1255–1332.

Wood, S.A., Crerar, D.A., Borcsik, M.P., 1987, Solubility of the assemblage pyrite-pyrrhotite-magnetite-sphalerite-galena-gold-stibnite-bismuthinite-argentite-molybdenite in H_2O-NaCl-CO_2 solutions from 200° to 350°C: Economic Geology, v. 82, p. 1864–1887.